Spatially Fixed and Moving Virtual Sensing Methods for Active Noise Control

Danielle J. Moreau

School of Mechanical Engineering
The University of Adelaide
South Australia 5005
Australia

A thesis submitted in fulfillment of the requirements
for the degree of Ph.D. in Mechanical Engineering
on 11 December 2009. Qualified on 12 February 2010.

References

Albertos, P., Goodwin, G. C., 2002. Virtual sensors for control applications. Annual Reviews in Control 26(1), 101–112.

Berkhoff, A. P., 2005. Control strategies for active noise barriers using near-field error sensing. Journal of the Acoustical Society of America 118(3), 1469–1479.

Brothanek, M., Jiricek, O., 2002. Formatting of zones of quiet around a head simulator. In: Proceedings of Active 2002. ISVR, Southampton, UK.

Bullmore, A. J., Nelson, P. A., Curtis, A. R. D., Elliott, S. J., 1987. The active minimisation of harmonic enclosed sound fields, Part II: A computer simulation. Journal of Sound and Vibration 117(1), 15–33.

Cazzolato, B. S., 1999. Sensing systems for active control of sound transmission into cavities. Ph.D. thesis, Department of Mechanical Engineering, The University of Adelaide, Australia.

Cazzolato, B. S., 2002. An adaptive LMS virtual microphone. In: Proceedings of Active 2002. ISVR, Southampton, UK, pp. 105–116.

Cazzolato, B. S., Ghan, J., 2005. Frequency domain expressions for the estimation of time-averaged acoustic energy density. Journal of the Acoustical Society of America 117(6), 3750–3756.

Cazzolato, B. S., Halim, D., Petersen, C. D., Kahana, Y., Kots, A., 2005a. An optical 3D sound intensity and energy density probe. In: Proceedings of Acoustics 2005. Busselton, Western Australia, Australia, pp. 101–106.

Cazzolato, B. S., Hansen, C. H., 2000a. Errors arising from three-dimensional energy density sensing in one-dimensional sound fields. Journal of Sound and Vibration 236(3), 375–400.

Cazzolato, B. S., Hansen, C. H., 2000b. Errors in the measurement of acoustic energy density in one-dimensional sound fields. Journal of Sound and Vibration 236(5), 801–831.

Cazzolato, B. S., Petersen, C. D., Howard, C. Q., Zander, A. C., 2005b. Active control of energy density in a one-dimensional waveguide: A cautionary note (L). Journal of the Acoustical Society of America 117(6), 3377–3380.

David, A., Elliott, S. J., 1994. Numerical studies of actively generated quiet zones. Applied Acoustics 41, 63–79.

de Bree, H. E., 1998. The microflown: A true particle velocity microphone; sound intensity application. NAG Journal 141(18).

de Bree, H. E., Druyvesteyn, W. F., Berenschot, E., Elwenspoek, M., 1999. Three dimensional sound intensity measurements using microflown particle velocity sensors. In: MEMs' 99. Orlando.

Diaz, J., Egana, J. M., Vinolas, J., 2006. A local active noise control system based on a virtual-microphone technique for railway sleeping vehicle applications. Mechanical Systems and Signal Processing 20, 2259–2276.

Elliott, S. J., 2001. Signal Processing for Active Control. Academic Press.

Elliott, S. J., Curtis, A. R. D., Bullmore, A. J., Nelson, P. A., 1987. The active minimisation of harmonic enclosed sound fields, Part III: Experimental verification. Journal of Sound and Vibration 117(1), 35–38.

Elliott, S. J., David, A., 1992. A virtual microphone arrangement for local active sound control. In: Proceedings of the 1st International Conference on Motion and Vibration Control. Yokohama, pp. 1027–1031.

Elliott, S. J., Garcia-Bonito, J., 1995. Active cancellation of pressure and pressure gradient in a diffuse sound field. Journal of Sound and Vibration 186(4), 696–704.

Elliott, S. J., Joseph, P., Bullmore, A. J., Nelson, P. A., 1988a. Active cancellation at a point in a pure tone diffuse sound field. Journal of Sound and Vibration 120(1), 183–189.

Elliott, S. J., Joseph, P., Nelson, P. A., 1988b. Active control in diffuse sound fields. Proceedings of the Institute of Acoustics 10(2), 605–614.

Elliott, S. J., Nelson, P. A., Stothers, I. M., Boucher, C. C., 1990. In-flight experiments on the active control of propeller-induced cabin noise. Journal of Sound and Vibration 140(2), 219–238.

Elliott, S. J., Stothers, I. M., Nelson, P. A., McDonald, A. M., Quinn, D. C., Saunders, T., 1998. The active control of engine noise inside cars. In: Proceedings of Inter-Noise 88. pp. 987–990.

Fahy, F., 1995. Sound Intensity, 2nd Edition. E&FN Spon.

Friot, E., Roure, A., Winninger, M., 2001. A simplified remote microphone technique for active noise control at virtual error sensors. In: Proceedings of Inter-Noise 01. The Hague, Netherlands.

Garcia-Bonito, J., Elliott, S. J., 1995a. Local active control of diffracted diffuse sound fields. Journal of the Acoustical Society of America 98(2), 1017–1024.

Garcia-Bonito, J., Elliott, S. J., 1995b. Strategies for local active control in diffuse sound fields. In: Proceedings of Active 1995. Newport Beach, CA, USA, pp. 561–572.

Garcia-Bonito, J., Elliott, S. J., 1999. Active cancellation of acoustic pressure and particle velocity in the near field of a source. Journal of Sound and Vibration 221(1), 85–116.

Garcia-Bonito, J., Elliott, S. J., Bonilha, M., 1997a. Active cancellation of pressure at a point in a pure tone diffracted diffuse sound field. Journal of Sound and Vibration 201(1), 43–65.

Garcia-Bonito, J., Elliott, S. J., Boucher, C. C., 1996. A virtual microphone arrangement in a practical active headrest. In: Proceedings of Inter-noise 96. pp. 1115–1120.

Garcia-Bonito, J., Elliott, S. J., Boucher, C. C., 1997b. Generation of zones of quiet using a virtual microphone arrangement. Journal of the Acoustical Society of America 101(6), 3498–3516.

Garcia-Bonito, J., Elliott, S. J., Boucher, C. C., 1997c. A novel secondary source for a local active noise control system. In: Proceedings of Active 1997. Budapest, Hungary, pp. 405–418.

Gawron, H. J., Schaaf, K., 1992. Interior car noise: Active cancellation of harmonics using virtual microphones. In: Proceedings of the 2nd International Conference on Vehicle Comfort: Ergonomic, Vibrational and Thermal Aspects. Bologna, Italy, pp. 739–748.

Ghan, J., Cazzolato, B. S., Snyder, S. D., 2003. Expression for the estimation of time-averaged acoustic energy density using the two-microphone method (l). Journal of the Acoustical Society of America 113(5), 2404–2407.

Ghan, J., Cazzolato, B. S., Snyder, S. D., 2004. Statistical errors in the estimation of time-averaged acoustic energy density using the two-microphone method. Journal of the Acoustical Society of America 115(3), 1179–1184.

Goodwin, G. C., 1999. Evaluating the performance of virtual sensors. In: Proceedings of Information, Decision and Control. pp. 5–12.

Hansen, C. H., 2001. Understanding Active Noise Cancellation. Spon Press.

Hansen, C. H., Synder, S. D., 1997. Active Control of Noise and Vibration. E & FN Spon.

Hashimoto, H., Terai, K., Kiba, M., Nakama, Y., 1995. Active noise control for seat audio system. In: Proceedings of Active 1995. Newport Beach, CA, USA, pp. 1279–1290.

Haverkamp, L. R. J., 2001. State space identification: Theory and practice. Ph.D. thesis, System and Control Engineering Group, Delft University of Technology.

Holmberg, U., Ramner, N., Slovak, R., 2002. Low complexity robust control of a headrest system based on virtual microphones and the internal model principle. In: Proceedings of Active 2002. ISVR, Southampton, UK, pp. 1243–1250.

Horihata, S., Matsuoka, S., Kitagawa, H., Ishimitsu, S., 1997. Active noise control by means of virtual error microphone system. In: Proceedings of Inter-Noise 97. Budapest, pp. 529–532.

Johansson, S., Persson, P., Claesson, I., 1999. Active control of propeller-induced noise in an aircraft mock-up. In: Proceedings of Active 1999. Florida, USA, pp. 741–752.

Joseph, P., Elliott, S. J., Nelson, P. A., 1994a. Near field zones of quiet. Journal of Sound and Vibration 172(5), 605–627.

Joseph, P., Elliott, S. J., Nelson, P. A., 1994b. Statistical aspects of active control in harmonic enclosed sound fields. Journal of Sound and Vibration 172(5), 629–655.

Kammer, D. C., 1997. Estimation of structural response using remote sensor locations. Journal of Guidance, Control, and Dynamics 20(3), 501–508.

Kestell, C. D., 2000. Active control of sound in a small single engine aircraft cabin with virtual error sensors. Ph.D. thesis, Department of Mechanical Engineering, The University of Adelaide, Australia.

Kestell, C. D., Cazzolato, B. S., Hansen, C. H., 2000a. Active noise control with virtual sensors in a long narrow duct. International Journal of Acoustics and Vibration 5(2), 63–76.

Kestell, C. D., Cazzolato, B. S., Hansen, C. H., 2000b. Virtual energy density sensing in active noise control systems. In: Proceedings of the 7th International Congress on Sound and Vibration. Garmisch-Partenkirchen, Germany.

Kestell, C. D., Cazzolato, B. S., Hansen, C. H., 2001a. Active noise control in a free field with virtual sensors. Journal of the Acoustical Society of America 109(1), 232–243.

Kestell, C. D., Cazzolato, B. S., Hansen, C. H., 2001b. Virtual sensors in active noise control. Acoustics Australia 29(2), 57–61.

Kreyszig, E., 1999. Advanced Engineering Mathematics, 8th Edition. John Wiley and Sons.

Kuo, S. M., 2006. Digital signal processing algorithms and implementations on active noise control systems. In: Proceedings of Active 2006. Adelaide, Australia.

Kuo, S. M., Gan, W. S., 2004. Active noise control systems with optimized secondary path. In: Proceedings of the 2004 IEEE International Conference on Control Applications. Taipei, Taiwan, pp. 765–770.

Kuo, S. M., Gan, W. S., Kalluri, S., 2003. Virtual sensor algorithms for active noise control systems. In: Proceedings of the 2003 IEEE International Symposium on Intelligent Signal Processing and Communication Systems (ISPACS 2003). Awaji Island, Japan, pp. 714–719.

Kuo, S. M., Gireddy, R., 2007. Real-time experiment of snore active noise control. In: Proceedings of the 16th IEEE International Conference on Control Applications. pp. 1342–1346.

Kuo, S. M., Morgan, D. R., 1996. Active Noise Control Systems, Algorithms and DSP Implementation. John Wiley and Sons, Inc.

Lockwood, M. E., Jones, D. L., 2006. Beamformer performance with acoustic velocity sensors in air. Journal of the Acoustical Society of America 119(1), 608–619.

Mathworks, 2007a. Getting Started with xPC Target. The Mathworks, Inc., Natick, MA.

Mathworks, 2007b. xPC Target User's Guide. The Mathworks, Inc., Natick, MA.

Matsuoka, S., Kitagawa, H., Horihata, S., Ishimitu, S., Tamura, F., 1996. Active noise control using a virtual error microphone system. Transactions of the Japan Society of Mechanical Engineers 62(601), 3459–3464.

Miyoshi, M., Kaneda, Y., 1991. Active control of broadband random noise in a reverberant three-dimensional space. Noise Control Engineering Journal 36(2), 85–90.

Morse, P. M., 1948. Vibration and Sound. McGraw-Hill, New York.

Munn, J. M., 2004. Virtual sensors for active noise control. Ph.D. thesis, Department of Mechanical Engineering, The University of Adelaide, Australia.

Munn, J. M., Cazzolato, B. S., Hansen, C. H., 2002a. Virtual sensing: Open loop vs adaptive LMS. In: Proceedings of Acoustics 2002. pp. 24–33.

Munn, J. M., Cazzolato, B. S., Hansen, C. H., 2003a. Virtual sensing using an adaptive LMS algorithm. In: Proceedings of Wespac 8: The 8th Western Pacific Acoustics Conference, Acoustics on the move. Melbourne, Australia.

Munn, J. M., Cazzolato, B. S., Hansen, C. H., Kestell, C. D., 2002b. Higher-order virtual sensing for remote active noise control. In: Proceedings of Active 2002. ISVR, Southampton, UK, pp. 377–386.

Munn, J. M., Cazzolato, B. S., Kestell, C. D., Hansen, C. H., 2003b. Virtual error sensing for active noise control in a one-dimensional waveguide: Performance prediction versus measurement. Journal of the Acoustical Society of America 113(1), 35–38.

Munn, J. M., Kestell, C. D., Cazzolato, B. S., Hansen, C. H., 2001a. Real-time feedforward active control using virtual sensors in a long narrow duct. In: Proceedings of Acoustics 2001. Canberra, Australia.

Munn, J. M., Kestell, C. D., Cazzolato, B. S., Hansen, C. H., 2001b. Real time feedforward active noise control using virtual sensors. In: Proceedings of the 2001 International Congress and Exhibition on Noise Control Engineering. The Hague, Netherlands.

Nelson, P. A., Curtis, A. R. D., Elliott, S. J., Bullmore, A. J., 1987. The active minimisation of harmonic enclosed sound fields, Part I: Theory. Journal of Sound and Vibration 117(1), 1–13.

Nelson, P. A., Elliott, S. J., 1992. Active Control of Sound, 1st Edition. Academic Press.

Olson, H. F., May, E. G., 1953. Electronic sound absorber. Journal of the Acoustical Society of America 25(6), 1130–1136.

Park, Y. C., Sommerfeldt, S. D., 1997. Global attenuation of broadband noise fields using energy density control. Journal of the Acoustical Society of America 101(1), 350–359.

Parkins, J. W., Sommerfeldt, S. D., Tichy, J., 2000. Error analysis of a practical energy density sensor. Journal of the Acoustical Society of America 108(1), 211–222.

Pascal, J., Li, J., 2008. A systematic method to obtain 3D finite-difference formulations for acoustic intensity and other energy quantities. Journal of Sound and Vibration 310(1), 1093–1111.

Pascal, J., Thomas, J., Jing-Fang, L., 2008. On the statistical errors in the estimate of acoustical energy density by using two microphones in a one dimensional field. Journal of the Acoustical Society of America 124(4), 2085–2089.

Pawelczyk, M., 2003a. A double input-quadruple output adaptive controller for the active headrest system. In: Active noise and vibration control methods conference. Cracow, Poland.

Pawelczyk, M., 2003b. Multiple input- multiple output adaptive feedback control strategies for the active headrest system: design and real-time implementation. International Journal of Adaptive Control and Signal Processing 17(10), 785–800.

Pawelczyk, M., 2003c. Noise control in the active headrest based on estimated residual signals at virtual microphones. In: Proceedings of the 10th International Congress on Sound and Vibration. Stockholm, Sweeden, pp. 251–258.

Pawelczyk, M., 2004a. Active noise control in a phone. In: Proceedings of the 11th International Congress on Sound and Vibration. St Petersburg, Russia, pp. 523–530.

Pawelczyk, M., 2004b. Adaptive noise control algorithms for active headrest system. Control Engineering Practice 12(9), 1101–1112.

Pawelczyk, M., 2005. Design and analysis of a virtual-microphone active noise control system. In: Proceedings of the 12th International Congress on Sound and Vibration. Lisbon, Portugal.

Pawelczyk, M., 2006. Polynomial approach to design of feedback virtual-microphone active noise control system. In: Proceedings of the 13th International Congress on Sound and Vibration. Vienna, Austria.

Petersen, C. D., 2007. Optimal spatially fixed and moving virtual sensing algorithms for local active noise control. Ph.D. thesis, School of Mechanical Engineering, The University of Adelaide, Australia.

Petersen, C. D., Cazzolato, B. S., Zander, A. C., Hansen, C. H., 2006. Active noise control at a moving location using virtual sensing. In: Proceedings of the 13th International Congress on Sound and Vibration. Vienna.

Petersen, C. D., Fraanje, R., Cazzolato, B. S., Zander, A. C., Hansen, C. H., 2008. A Kalman filter approach to virtual sensing for active noise control. Mechanical Systems and Signal Processing 22(2), 490–508, submitted to Elsevier Science.

Petersen, C. D., Zander, A. C., Cazzolato, B. S., Hansen, C. H., 2005. Optimal virtual sensing for active noise control in a rigid-walled acoustic duct. Journal of the Acoustical Society of America 118(5), 3086–3093.

Petersen, C. D., Zander, A. C., Cazzolato, B. S., Hansen, C. H., 2007. A moving zone of quiet for narrowband noise in a one-dimensional duct using virtual sensing. Journal of the Acoustical Society of America 121(3), 1459–1470.

Popovich, S. R., 1997. Active acoustic control in remote regions. US Patent No 5,701,350.

Radcliffe, C. J., Gogate, S. D., 1993. A model based feedforward noise control algorithm for vehicle interiors. Advanced Automotive Technologies ASME 52(DSC), 299–304.

Rafaely, B., 2000. Spatial-temporal correlation of a diffuse sound field. Journal of the Acoustical Society of America 107(6), 3254–3258.

Rafaely, B., 2001. Zones of quiet in a broadband diffuse sound field. Journal of the Acoustical Society of America 110(1), 296–302.

Rafaely, B., Elliott, S. J., 1999. H_2/H_∞ active control of sound in a headrest: Design and implementation. IEEE Transactions on Control Systems Technology 7(1), 79–84.

Rafaely, B., Elliott, S. J., Garcia-Bonito, J., 1999. Broadband performance of an active headrest. Journal of the Acoustical Society of America 106(2), 787–793.

Rafaely, B., Garcia-Bonito, J., Elliott, S. J., 1997. Feedback control of sound in headrest. In: Proceedings of Active 1997. Budapest, pp. 445–456.

Renault, S., Rymeyko, F., Berry, A., 2000. Active noise control in enclosure with virtual microphone. Canadian Acoustics 28(3), 72–73.

Roure, A., Albarrazin, A., 1999. The remote microphone technique for active noise control. In: Proceedings of Active 1999. Florida, USA, pp. 1233–1244.

Schroeder, M. R., 1996. The "Schroeder frequency" revisited. Journal of the Acoustical Society of America 99(5), 3240–3241.

Schroeder, M. R., Kuttruff, K. H., 1962. On frequency response curves in rooms, comparison of experimental, theoretical and Monte Carlo results for the average frequency spacing between maxima. Journal of the Acoustical Society of America 34(1), 76–80.

Skogestad, S., Postlethwaite, I., 2005. Multivariable Feedback Control: Analysis and Design. John Wiley.

Sommerfeldt, S. D., 2006. Using energy-based control to achieve global attenuation. In: Proceedings of Active 2006. Adelaide, Australia.

Sommerfeldt, S. D., Nashif, P. J., 1991. A comparison of control strategies for minimising the sound field in enclosures. In: Proceedings of Noise-Control Engineering. pp. 299–306.

Sommerfeldt, S. D., Nashif, P. J., 1992. Energy based control of the sound field in enclosures. In: Proceedings of the Second International Congress on Recent Developments in Air- and Structure-borne Sound and Vibration. Auburn University, USA, pp. 361–368.

Sommerfeldt, S. D., Nashif, P. J., 1994. An adaptive filtered-x algorithm for energy based active control. Journal of the Acoustical Society of America 96(1), 300–305.

Sommerfeldt, S. D., Parkins, J. W., 1994. An evaluation of active noise attenuation in rectangular enclosures. In: Proceedings of Inter-Noise 94. Yokohama, pp. 1351–1356.

Sommerfeldt, S. D., Parkins, J. W., Park, Y. C., 1995. Global active noise control in rectangular enclosures. In: Proceedings of Active 1995. CA, USA, pp. 477–488.

Thanigai, P., Kuo, S. M., 2007. Intrauterine acoustics embedded active noise controller. In: Proceedings of the 16th IEEE International Conference on Control Applications. pp. 1359–1364.

World Health Organization, 1995. Who guidelines for community noise - a complete, authoritative guide on the effects of noise pollution on health.
URL `http://www.ruidos.org/Noise/WHO_Noise_guidelines_3.html`

World Health Organization, 2001. Occupational and community noise, fact sheet no. 258.
URL `http://www.who.int/mediacentre/factsheets/fs258/en/`

Yeh, R. Z., 1973. Modern probability theory. Harper and Row.

Yuan, J., 2004. Virtual sensing for broadband noise control in a lightly damped enclosure. Journal of the Acoustical Society of America 116(2), 934–941.

Zou, H., Qiu, X., 2008. Performance analysis of the virtual sound barrier system with a diffracting sphere. Applied Acoustics 69(10), 875–883.

Zou, H., Qiu, X., Lu, J., Niu, F., 2007. A preliminary experimental study on virtual sound barrier system. Journal of Sound and Vibration 307(1), 379–385.

Appendix A

Theoretical Lower Bounds on Control Performance with the Stochastically Optimal Tonal Diffuse Field (SOTDF) Virtual Sensing Method

A.1 Cancelling the pressure at a virtual location with one secondary source using the measured pressure and pressure gradient at a point

An expression for the lower bound on control performance can be derived when the pressure at the virtual location is minimised with a single secondary source. This expression gives the worst case limit on the expected control performance.

When a single secondary source is used to cancel the pressure at the virtual location, $\hat{p}(\mathbf{x}_0)$, $\mathbf{H}_p(\mathbf{x}_0)\mathbf{p} = 0$. Therefore,

$$\begin{aligned} p(\mathbf{x}) &= \mathbf{H}_p(\mathbf{x})\mathbf{p} + p_u(\mathbf{x}) \\ &= \mathbf{H}_p(\mathbf{x})\mathbf{p} + \lambda\mathbf{H}_p(\mathbf{x}_0)\mathbf{p} + p_u(\mathbf{x}), \end{aligned} \tag{A.1}$$

where $\lambda \in \mathbb{R}$. Consequently

$$p(\mathbf{x}) = [\mathrm{H}_{pp1}(\mathbf{x}) + \lambda \mathrm{H}_{pp1}(\mathbf{x}_0)\mathrm{H}_{pg1}(\mathbf{x}) + \lambda \mathrm{H}_{pg1}(\mathbf{x}_0)]\mathbf{p} + p_u(\mathbf{x}). \tag{A.2}$$

In order to make the coefficient of $g(\mathbf{x}_1)$ in $\mathbf{p}$ equal to zero in Eq. (A.2), λ is selected to be

$-\mathrm{H}_{pg1}(\mathbf{x})/\mathrm{H}_{pg1}(\mathbf{x}_0)$. Then

$$p(\mathbf{x}) = \frac{\mathrm{H}_{pp1}(\mathbf{x})\mathrm{H}_{pg1}(\mathbf{x}_0) - \mathrm{H}_{pg1}(\mathbf{x})\mathrm{H}_{pp1}(\mathbf{x}_0)}{\mathrm{H}_{pg1}(\mathbf{x}_0)} p(\mathbf{x}_1) + p_u(\mathbf{x}). \tag{A.3}$$

Multiplying this expression by its conjugate and spatially averaging yields

$$\left\langle |p(\mathbf{x})|^2 \right\rangle = \left(\frac{\mathrm{H}_{pp1}(\mathbf{x})\mathrm{H}_{pg1}(\mathbf{x}_0) - \mathrm{H}_{pg1}(\mathbf{x})\mathrm{H}_{pp1}(\mathbf{x}_0)}{\mathrm{H}_{pg1}(\mathbf{x}_0)} \right)^2 \left\langle |p(\mathbf{x}_1)|^2 \right\rangle + \left\langle |p_u(\mathbf{x})|^2 \right\rangle. \tag{A.4}$$

Eq. (3.42) may now be used to give the mean squared level of the uncorrelated pressure component as

$$\begin{aligned} \left\langle |p(\mathbf{x})|^2 \right\rangle &= \left(\frac{A(\mathbf{x}-\mathbf{x}_1)B(\mathbf{x}_0-\mathbf{x}_1) - B(\mathbf{x}-\mathbf{x}_1)A(\mathbf{x}_0-\mathbf{x}_1)}{B(\mathbf{x}_0-\mathbf{x}_1)} \right)^2 \left\langle |p(\mathbf{x}_1)|^2 \right\rangle \\ &\quad + \left(1 - A^2(\mathbf{x}-\mathbf{x}_1) - \frac{3}{k^2} B^2(\mathbf{x}-\mathbf{x}_1) \right) \left\langle |p|^2 \right\rangle. \end{aligned} \tag{A.5}$$

The quadratic mean/arithmetic mean inequality can be used to give the limit on control performance at a point $\mathbf{x}$ using

$$\left\langle |p(\mathbf{x})|^2 \right\rangle \leq n \sum_i \left\langle |p_i(\mathbf{x})|^2 \right\rangle = n \sum_i \left\langle |p_i|^2 \right\rangle = n \left\langle |p|^2 \right\rangle, \tag{A.6}$$

where n is the number of diffuse fields comprising the total diffuse sound field. In this case, a single secondary source is used and therefore

$$\left\langle |p(\mathbf{x}_1)|^2 \right\rangle \leq 2 \left\langle |p|^2 \right\rangle. \tag{A.7}$$

Therefore the worst case limit on control performance at a point $\mathbf{x}$ in the controlled

sound field is given by

$$\left\langle |p(\mathbf{x})|^2 \right\rangle \leq \left[2 \left(\frac{A(\mathbf{x}-\mathbf{x}_1)B(\mathbf{x}_0-\mathbf{x}_1) - B(\mathbf{x}-\mathbf{x}_1)A(\mathbf{x}_0-\mathbf{x}_1)}{B(\mathbf{x}_0-\mathbf{x}_1)} \right)^2 + \left(1 - A^2(\mathbf{x}-\mathbf{x}_1) - \frac{3}{k^2} B^2(\mathbf{x}-\mathbf{x}_1) \right) \right] \left\langle |p|^2 \right\rangle . \quad \text{(A.8)}$$

Therefore the worst case limit on relative control performance at the point $\mathbf{x}$ is given by

$$\frac{\left\langle |p(\mathbf{x})|^2 \right\rangle}{\left\langle |p_p(\mathbf{x})|^2 \right\rangle} \leq \left[2 \left(\frac{A(\mathbf{x}-\mathbf{x}_1)B(\mathbf{x}_0-\mathbf{x}_1) - B(\mathbf{x}-\mathbf{x}_1)A(\mathbf{x}_0-\mathbf{x}_1)}{B(\mathbf{x}_0-\mathbf{x}_1)} \right)^2 + \left(1 - A^2(\mathbf{x}-\mathbf{x}_1) - \frac{3}{k^2} B^2(\mathbf{x}-\mathbf{x}_1) \right) \right] \alpha. \quad \text{(A.9)}$$

The expression for the mean squared pressure at a point $\mathbf{x}$ in the controlled sound field given in Eq. (A.5) is greater than or equal to the expression in Eq. (3.42) for the mean squared pressure at $\mathbf{x}$ when cancelling the pressure and pressure gradient at $\mathbf{x}_1$ with two control sources. The two expressions are equal when $\mathbf{x} = \mathbf{x}_0$ and the mean squared pressure at the point $\mathbf{x}_0$ becomes

$$\left\langle |p(\mathbf{x}_0)|^2 \right\rangle = \left(1 - A^2(\mathbf{x}_0-\mathbf{x}_1) - \frac{3}{k^2} B^2(\mathbf{x}_0-\mathbf{x}_1) \right) \left\langle |p|^2 \right\rangle . \quad \text{(A.10)}$$

In the case that $\mathbf{x}_0 = \mathbf{x}_1$, then $\hat{p}(\mathbf{x}_0) = p(\mathbf{x}_1)$ and this control strategy is equivalent to control strategy 1, minimising the pressure at a point with a single control source.

A.2 Cancelling the pressure at a virtual location with one secondary source using the measured pressures at two points

Following the same method as in Section A.1, the worst case limit on control performance at a point $\mathbf{x}$ in the controlled sound field can be found. If a single secondary source is used to drive $\hat{p}(\mathbf{x}_0)$ to zero, it can be shown that

$$\left\langle |p(\mathbf{x})|^2 \right\rangle = \left(\frac{\mathrm{H}_{pp1}(\mathbf{x})\mathrm{H}_{pp2}(\mathbf{x}_0) - \mathrm{H}_{pp2}(\mathbf{x})\mathrm{H}_{pp1}(\mathbf{x}_0)}{\mathrm{H}_{pp2}(\mathbf{x}_0)} \right)^2 \left\langle |p(\mathbf{x}_1)|^2 \right\rangle + \left\langle |p_u(\mathbf{x})|^2 \right\rangle . \quad \text{(A.11)}$$

Eq. (3.48) may now be used to give the mean squared level of the uncorrelated pressure component as

$$\begin{aligned}\left\langle |p(\mathbf{x})|^2 \right\rangle &= \left(\frac{A(\mathbf{x}-\mathbf{x}_1)A(\mathbf{x}_0-\mathbf{x}_2) - A(\mathbf{x}-\mathbf{x}_2)A(\mathbf{x}_0-\mathbf{x}_1)}{A(\mathbf{x}_0-\mathbf{x}_2) - A(\mathbf{x}_1-\mathbf{x}_2)A(\mathbf{x}_0-\mathbf{x}_1)} \right)^2 \left\langle |p(\mathbf{x}_1)|^2 \right\rangle \\ &\quad + \left(1 - \frac{A^2(\mathbf{x}-\mathbf{x}_1) + A^2(\mathbf{x}-\mathbf{x}_2) - 2A(\mathbf{x}-\mathbf{x}_1)A(\mathbf{x}-\mathbf{x}_2)A(\mathbf{x}_1-\mathbf{x}_2)}{1 - A^2(\mathbf{x}_1-\mathbf{x}_2)} \right) \left\langle |p|^2 \right\rangle . \end{aligned} \tag{A.12}$$

Once again, a single secondary source is used and therefore

$$\left\langle |p(\mathbf{x}_1)|^2 \right\rangle \leq 2 \left\langle |p|^2 \right\rangle . \tag{A.13}$$

Therefore the worst case limit on control performance at a point $\mathbf{x}$ is given by

$$\begin{aligned}\left\langle |p(\mathbf{x})|^2 \right\rangle &\leq \left[2 \left(\frac{A(\mathbf{x}-\mathbf{x}_1)A(\mathbf{x}_0-\mathbf{x}_2) - A(\mathbf{x}-\mathbf{x}_2)A(\mathbf{x}_0-\mathbf{x}_1)}{A(\mathbf{x}_0-\mathbf{x}_2) - A(\mathbf{x}_1-\mathbf{x}_2)A(\mathbf{x}_0-\mathbf{x}_1)} \right)^2 \right. \\ &\quad \left. + \left(1 - \frac{A^2(\mathbf{x}-\mathbf{x}_1) + A^2(\mathbf{x}-\mathbf{x}_2) - 2A(\mathbf{x}-\mathbf{x}_1)A(\mathbf{x}-\mathbf{x}_2)A(\mathbf{x}_1-\mathbf{x}_2)}{1 - A^2(\mathbf{x}_1-\mathbf{x}_2)} \right) \right] \left\langle |p|^2 \right\rangle . \end{aligned} \tag{A.14}$$

The worst case limit on relative control performance at the point $\mathbf{x}$ is given by

$$\begin{aligned}\frac{\left\langle |p(\mathbf{x})|^2 \right\rangle}{\left\langle |p_p(\mathbf{x})|^2 \right\rangle} &\leq \left[2 \left(\frac{A(\mathbf{x}-\mathbf{x}_1)A(\mathbf{x}_0-\mathbf{x}_2) - A(\mathbf{x}-\mathbf{x}_2)A(\mathbf{x}_0-\mathbf{x}_1)}{A(\mathbf{x}_0-\mathbf{x}_2) - A(\mathbf{x}_1-\mathbf{x}_2)A(\mathbf{x}_0-\mathbf{x}_1)} \right)^2 \right. \\ &\quad \left. + \left(1 - \frac{A^2(\mathbf{x}-\mathbf{x}_1) + A^2(\mathbf{x}-\mathbf{x}_2) - 2A(\mathbf{x}-\mathbf{x}_1)A(\mathbf{x}-\mathbf{x}_2)A(\mathbf{x}_1-\mathbf{x}_2)}{1 - A^2(\mathbf{x}_1-\mathbf{x}_2)} \right) \right] \alpha . \end{aligned} \tag{A.15}$$

A.3 Cancelling the pressure and pressure gradient at a virtual location with two secondary sources using the measured pressures and pressure gradients at two points

If two secondary sources are used to drive $\hat{p}(\mathbf{x}_0)$ and $\hat{g}(\mathbf{x}_0)$ to zero, then the procedure outlined in Section A.1 can be used to derive the worst case limit on control

performance at a point $\mathbf{x}$. Using $\mathrm{H}_p(\mathbf{x})$ and $\mathrm{H}_g(\mathbf{x})$ as defined in Eqs. (3.104) and (3.105) and Eq. (3.53) for the mean squared pressure at a point when cancelling the pressures and pressure gradients at two points with four control sources, the worst case limit on control performance at a point $\mathbf{x}$ is

$$\begin{aligned}\left\langle |p(\mathbf{x})|^2 \right\rangle \;\leq\; & \Bigg[3\Bigg(\Bigg(\mathrm{H}_{pp1}(\mathbf{x}) - \left(\frac{\mathrm{H}_{pp1}(\mathbf{x}_0)\mathrm{H}_{gg2}(\mathbf{x}_0) - \mathrm{H}_{gp1}(\mathbf{x}_0)\mathrm{H}_{pg2}(\mathbf{x}_0)}{\mathrm{H}_{pp2}(\mathbf{x}_0)\mathrm{H}_{gg2}(\mathbf{x}_0) - \mathrm{H}_{gp2}(\mathbf{x}_0)\mathrm{H}_{pg2}(\mathbf{x}_0)}\right)\mathrm{H}_{pp2}(\mathbf{x}) \\ & - \left(-\frac{\mathrm{H}_{pp1}(\mathbf{x}_0)\mathrm{H}_{gp2}(\mathbf{x}_0) - \mathrm{H}_{gp1}(\mathbf{x}_0)\mathrm{H}_{pp2}(\mathbf{x}_0)}{\mathrm{H}_{pp2}(\mathbf{x}_0)\mathrm{H}_{gg2}(\mathbf{x}_0) - \mathrm{H}_{gp2}(\mathbf{x}_0)\mathrm{H}_{pg2}(\mathbf{x}_0)}\right)\mathrm{H}_{pg2}(\mathbf{x})\Bigg)^2 \\ & + \frac{k^2}{3}\Bigg(\mathrm{H}_{pg1}(\mathbf{x}) - \left(\frac{\mathrm{H}_{pg1}(\mathbf{x}_0)\mathrm{H}_{gg2}(\mathbf{x}_0) - \mathrm{H}_{gg1}(\mathbf{x}_0)\mathrm{H}_{pg2}(\mathbf{x}_0)}{\mathrm{H}_{pp2}(\mathbf{x}_0)\mathrm{H}_{gg2}(\mathbf{x}_0) - \mathrm{H}_{gp2}(\mathbf{x}_0)\mathrm{H}_{pg2}(\mathbf{x}_0)}\right)\mathrm{H}_{pp2}(\mathbf{x}) \\ & - \left(-\frac{\mathrm{H}_{pg1}(\mathbf{x}_0)\mathrm{H}_{gp2}(\mathbf{x}_0) - \mathrm{H}_{gg1}(\mathbf{x}_0)\mathrm{H}_{pp2}(\mathbf{x}_0)}{\mathrm{H}_{pp2}(\mathbf{x}_0)\mathrm{H}_{gg2}(\mathbf{x}_0) - \mathrm{H}_{gp2}(\mathbf{x}_0)\mathrm{H}_{pg2}(\mathbf{x}_0)}\right)\mathrm{H}_{pg2}(\mathbf{x})\Bigg)^2\Bigg) \\ & + \left(1 - \mathbf{L}_p(\mathbf{x})\mathbf{M}^{-\mathbf{1}}\mathbf{L}_p^H(\mathbf{x})\right)\Bigg]\left\langle |p|^2 \right\rangle. \end{aligned} \tag{A.16}$$

The worst case limit on relative control performance at the point $\mathbf{x}$ is given by

$$\begin{aligned}\frac{\left\langle |p(\mathbf{x})|^2 \right\rangle}{\left\langle |p_p(\mathbf{x})|^2 \right\rangle} \;\leq\; & \Bigg[3\Bigg(\Bigg(\mathrm{H}_{pp1}(\mathbf{x}) - \left(\frac{\mathrm{H}_{pp1}(\mathbf{x}_0)\mathrm{H}_{gg2}(\mathbf{x}_0) - \mathrm{H}_{gp1}(\mathbf{x}_0)\mathrm{H}_{pg2}(\mathbf{x}_0)}{\mathrm{H}_{pp2}(\mathbf{x}_0)\mathrm{H}_{gg2}(\mathbf{x}_0) - \mathrm{H}_{gp2}(\mathbf{x}_0)\mathrm{H}_{pg2}(\mathbf{x}_0)}\right)\mathrm{H}_{pp2}(\mathbf{x}) \\ & - \left(-\frac{\mathrm{H}_{pp1}(\mathbf{x}_0)\mathrm{H}_{gp2}(\mathbf{x}_0) - \mathrm{H}_{gp1}(\mathbf{x}_0)\mathrm{H}_{pp2}(\mathbf{x}_0)}{\mathrm{H}_{pp2}(\mathbf{x}_0)\mathrm{H}_{gg2}(\mathbf{x}_0) - \mathrm{H}_{gp2}(\mathbf{x}_0)\mathrm{H}_{pg2}(\mathbf{x}_0)}\right)\mathrm{H}_{pg2}(\mathbf{x})\Bigg)^2 \\ & + \frac{k^2}{3}\Bigg(\mathrm{H}_{pg1}(\mathbf{x}) - \left(\frac{\mathrm{H}_{pg1}(\mathbf{x}_0)\mathrm{H}_{gg2}(\mathbf{x}_0) - \mathrm{H}_{gg1}(\mathbf{x}_0)\mathrm{H}_{pg2}(\mathbf{x}_0)}{\mathrm{H}_{pp2}(\mathbf{x}_0)\mathrm{H}_{gg2}(\mathbf{x}_0) - \mathrm{H}_{gp2}(\mathbf{x}_0)\mathrm{H}_{pg2}(\mathbf{x}_0)}\right)\mathrm{H}_{pp2}(\mathbf{x}) \\ & - \left(-\frac{\mathrm{H}_{pg1}(\mathbf{x}_0)\mathrm{H}_{gp2}(\mathbf{x}_0) - \mathrm{H}_{gg1}(\mathbf{x}_0)\mathrm{H}_{pp2}(\mathbf{x}_0)}{\mathrm{H}_{pp2}(\mathbf{x}_0)\mathrm{H}_{gg2}(\mathbf{x}_0) - \mathrm{H}_{gp2}(\mathbf{x}_0)\mathrm{H}_{pg2}(\mathbf{x}_0)}\right)\mathrm{H}_{pg2}(\mathbf{x})\Bigg)^2\Bigg) \\ & + \left(1 - \mathbf{L}_p(\mathbf{x})\mathbf{M}^{-\mathbf{1}}\mathbf{L}_p^H(\mathbf{x})\right)\Bigg]\alpha. \end{aligned} \tag{A.17}$$

A.4 Cancelling the pressure and pressure gradient at a virtual location with two secondary sources using the measured pressures at four points

If two secondary sources are used to drive $\hat{p}(\mathbf{x}_0)$ and $\hat{g}(\mathbf{x}_0)$ to zero, then the procedure outlined in Section A.1 can be used to derive the worst case limit on control performance at a point $\mathbf{x}$. Using $\mathrm{H}_p(\mathbf{x}_0)$ and $\mathrm{H}_g(\mathbf{x}_0)$ as defined in Eqs. (3.133) and

(3.134) and Eq. (3.58) for the mean squared pressure at a point when cancelling the pressures at four points with four control sources, the worst case limit on control performance at a point $\mathbf{x}$ is

$$\begin{aligned}\left\langle |p(\mathbf{x})|^2 \right\rangle \leq \Bigg[& 3 \Bigg(\Bigg(\mathrm{H}_{pp1}(\mathbf{x}) - \left(\frac{-\mathrm{H}_{pp1}(\mathbf{x}_0)\mathrm{H}_{gp4}(\mathbf{x}_0) + \mathrm{H}_{gp1}(\mathbf{x}_0)\mathrm{H}_{pp4}(\mathbf{x}_0)}{-\mathrm{H}_{pp3}(\mathbf{x}_0)\mathrm{H}_{gp4}(\mathbf{x}_0) + \mathrm{H}_{gp3}(\mathbf{x}_0)\mathrm{H}_{pp4}(\mathbf{x}_0)} \right) \mathrm{H}_{pp3}(\mathbf{x}) \\ & - \left(\frac{\mathrm{H}_{pp1}(\mathbf{x}_0)\mathrm{H}_{gp2}(\mathbf{x}_0) - \mathrm{H}_{gp1}(\mathbf{x}_0)\mathrm{H}_{pp2}(\mathbf{x}_0)}{-\mathrm{H}_{pp3}(\mathbf{x}_0)\mathrm{H}_{gp4}(\mathbf{x}_0) + \mathrm{H}_{gp3}(\mathbf{x}_0)\mathrm{H}_{pp4}(\mathbf{x}_0)} \right) \mathrm{H}_{pp4}(\mathbf{x}) \Bigg)^2 \\ & + \frac{k^2}{3} \Bigg(\mathrm{H}_{pp2}(\mathbf{x}) - \left(\frac{-\mathrm{H}_{pp2}(\mathbf{x}_0)\mathrm{H}_{gp4}(\mathbf{x}_0) + \mathrm{H}_{gp2}(\mathbf{x}_0)\mathrm{H}_{pp4}(\mathbf{x}_0)}{-\mathrm{H}_{pp3}(\mathbf{x}_0)\mathrm{H}_{gp4}(\mathbf{x}_0) + \mathrm{H}_{gp3}(\mathbf{x}_0)\mathrm{H}_{pp4}(\mathbf{x}_0)} \right) \mathrm{H}_{pp3}(\mathbf{x}) \\ & - \left(\frac{\mathrm{H}_{pp2}(\mathbf{x}_0)\mathrm{H}_{gp3}(\mathbf{x}_0) - \mathrm{H}_{gp2}(\mathbf{x}_0)\mathrm{H}_{pp3}(\mathbf{x}_0)}{-\mathrm{H}_{pp3}(\mathbf{x}_0)\mathrm{H}_{gp4}(\mathbf{x}_0) + \mathrm{H}_{gp3}(\mathbf{x}_0)\mathrm{H}_{pp4}(\mathbf{x}_0)} \right) \mathrm{H}_{pp4}(\mathbf{x}) \Bigg)^2 \Bigg) \\ & + \left(1 - \mathbf{L}_p(\mathbf{x})\mathbf{M}^{-\mathbf{1}}\mathbf{L}_p^H(\mathbf{x}) \right) \Big] \left\langle |p|^2 \right\rangle . \end{aligned} \tag{A.18}$$

The worst case limit on relative control performance at the point $\mathbf{x}$ is given by

$$\begin{aligned}\frac{\left\langle |p(\mathbf{x})|^2 \right\rangle}{\left\langle |p_p(\mathbf{x})|^2 \right\rangle} \leq \Bigg[& 3 \Bigg(\Bigg(\mathrm{H}_{pp1}(\mathbf{x}) - \left(\frac{-\mathrm{H}_{pp1}(\mathbf{x}_0)\mathrm{H}_{gp4}(\mathbf{x}_0) + \mathrm{H}_{gp1}(\mathbf{x}_0)\mathrm{H}_{pp4}(\mathbf{x}_0)}{-\mathrm{H}_{pp3}(\mathbf{x}_0)\mathrm{H}_{gp4}(\mathbf{x}_0) + \mathrm{H}_{gp3}(\mathbf{x}_0)\mathrm{H}_{pp4}(\mathbf{x}_0)} \right) \mathrm{H}_{pp3}(\mathbf{x}) \\ & - \left(\frac{\mathrm{H}_{pp1}(\mathbf{x}_0)\mathrm{H}_{gp2}(\mathbf{x}_0) - \mathrm{H}_{gp1}(\mathbf{x}_0)\mathrm{H}_{pp2}(\mathbf{x}_0)}{-\mathrm{H}_{pp3}(\mathbf{x}_0)\mathrm{H}_{gp4}(\mathbf{x}_0) + \mathrm{H}_{gp3}(\mathbf{x}_0)\mathrm{H}_{pp4}(\mathbf{x}_0)} \right) \mathrm{H}_{pp4}(\mathbf{x}) \Bigg)^2 \\ & + \frac{k^2}{3} \Bigg(\mathrm{H}_{pp2}(\mathbf{x}) - \left(\frac{-\mathrm{H}_{pp2}(\mathbf{x}_0)\mathrm{H}_{gp4}(\mathbf{x}_0) + \mathrm{H}_{gp2}(\mathbf{x}_0)\mathrm{H}_{pp4}(\mathbf{x}_0)}{-\mathrm{H}_{pp3}(\mathbf{x}_0)\mathrm{H}_{gp4}(\mathbf{x}_0) + \mathrm{H}_{gp3}(\mathbf{x}_0)\mathrm{H}_{pp4}(\mathbf{x}_0)} \right) \mathrm{H}_{pp3}(\mathbf{x}) \\ & - \left(\frac{\mathrm{H}_{pp2}(\mathbf{x}_0)\mathrm{H}_{gp3}(\mathbf{x}_0) - \mathrm{H}_{gp2}(\mathbf{x}_0)\mathrm{H}_{pp3}(\mathbf{x}_0)}{-\mathrm{H}_{pp3}(\mathbf{x}_0)\mathrm{H}_{gp4}(\mathbf{x}_0) + \mathrm{H}_{gp3}(\mathbf{x}_0)\mathrm{H}_{pp4}(\mathbf{x}_0)} \right) \mathrm{H}_{pp4}(\mathbf{x}) \Bigg)^2 \Bigg) \\ & + \left(1 - \mathbf{L}_p(\mathbf{x})\mathbf{M}^{-\mathbf{1}}\mathbf{L}_p^H(\mathbf{x}) \right) \Big] \alpha. \end{aligned} \tag{A.19}$$

Appendix B

Experimental Results of Active Noise Control with the Moving Virtual Microphone Methods in a Three-dimensional Sound Field

The real-time experimental results of active noise control at a moving virtual microphone located at the ear of a rotating artificial head were summarised in Chapter 4 for brevity. Further discussion of the experimental results obtained with the remote moving microphone technique, the adaptive LMS moving virtual microphone technique and the Stochastically Optimal Tonal Diffuse Field (SOTDF) moving virtual sensing method are presented as follows.

B.1 The remote moving microphone technique for a three-dimensional sound field

Figs. B.1 and B.2 (Figs. 4.10 and 4.11 in Section 4.3.1) show the attenuation achieved at the moving virtual location with the remote moving microphone technique at the 525 Hz resonance and off resonance at 510 Hz respectively. Control profiles are shown for active noise control at the moving virtual microphone, a fixed virtual microphone located at the ear of the artificial head when $\theta_h = 0°$, and the fixed physical microphone. The control performance at the ear of the artificial head is shown for the period of head rotation of $t_v = 10$ s in part (a) of Figs. B.1 and B.2 and $t_v = 5$ s in part (b) of Figs. B.1 and B.2. Part (c) of Figs. B.1 and B.2 shows

the desired trajectory of the artificial head and of the moving virtual microphone, in degrees, compared to the actual controlled head position. The transient behaviour seen in Figs. B.1 and B.2 at time $t/t_v = 0$ s, for both $t_v = 5$ s and $t_v = 10$ s, is caused by the controller initialising.

At the 525 Hz resonance with $t_v = 10$ s, active noise control at the moving virtual microphone achieves between 28 dB and 39 dB of attenuation at the ear of the artificial head, as shown in Fig. B.1 (a). Minimising the fixed virtual error signal achieves a maximum attenuation of 28 dB at the ear of the artificial head when $\theta_h = 0°$ and a minimum attenuation of 9 dB when $\theta_h = 45°$. Similarly, active noise control at the physical microphone achieves 22 dB of attenuation at the ear of the artificial head when $\theta_h = 0°$ and only 6 dB of attenuation when $\theta_h = 45°$. When the period of head rotation is reduced to $t_v = 5$ s, Fig. B.1 (b) shows that minimising the moving virtual error signal results in attenuation of between 20 dB and 35 dB being achieved at the ear of the artificial head. This is a significant improvement in control performance compared to active noise control at either the fixed virtual or physical microphone where attenuation levels again fall to 9 dB and 6 dB respectively when $\theta_h = 45°$.

Off resonance, with $t_v = 10$ s, active noise control at the moving virtual microphone achieves an attenuation of between 20 dB and 40 dB at the ear of the artificial head, as shown in Fig. B.2 (a). Minimising the fixed virtual error signal achieves a maximum attenuation of 29 dB at the ear of the artificial head when $\theta_h = 0°$ and a minimum attenuation of 9 dB when $\theta_h = 45°$. Active noise control at the physical microphone results in 18 dB of attenuation at the ear of the artificial head when $\theta_h = 0°$ and only 2 dB of attenuation when $\theta_h = 45°$. When the period of head rotation is reduced to $t_v = 5$ s, Fig. B.2 (b) shows an expected reduction in control performance. Minimising the moving virtual error signal results in attenuation of between 20 dB and 35 dB being achieved at the ear of the artificial head. This is still a significant improvement in control performance compared to active noise control at either the fixed virtual or physical microphone where the minimum attenuation levels are 7 dB and 2 dB respectively when $\theta_h = 45°$.

B.1.1 Robustness of the remote moving microphone technique for a three-dimensional sound field

Figs. B.3 and B.4 (Figs. 4.12 and 4.13 in Section 4.3.1.1) show the performance of the active noise control system in generating a zone of quiet at the virtual microphone

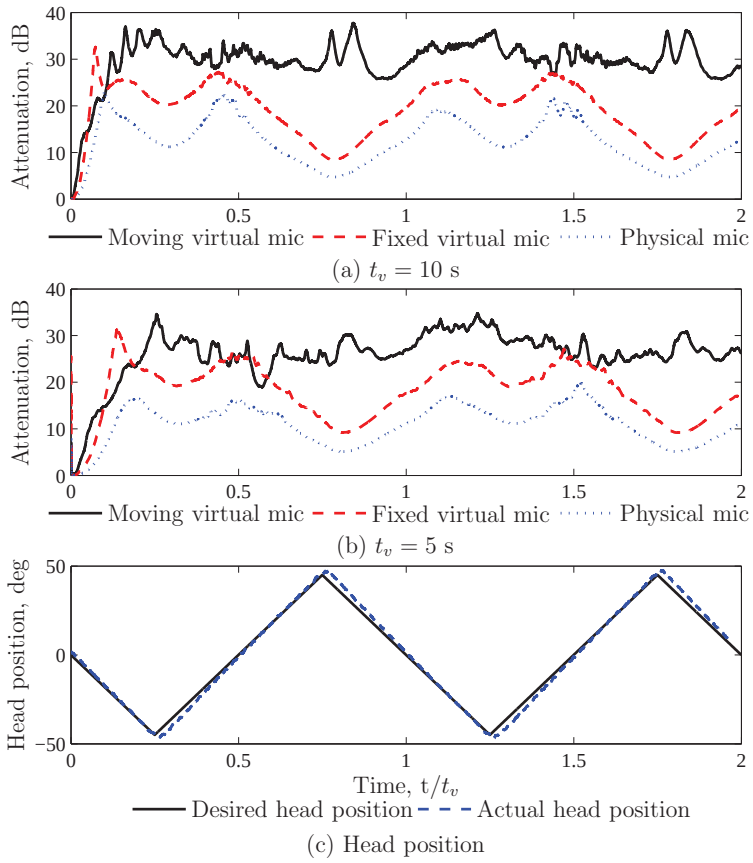

Figure B.1: Tonal attenuation achieved at the 525 Hz resonance with the remote moving microphone technique for a three-dimensional sound field. Control profiles are shown for active noise control at the moving virtual microphone, a virtual microphone spatially fixed at $\theta = 0°$, and the physical microphone, for a period of rotation (a) $t_v = 10$ s; (b) $t_v = 5$ s; and (c) head position.

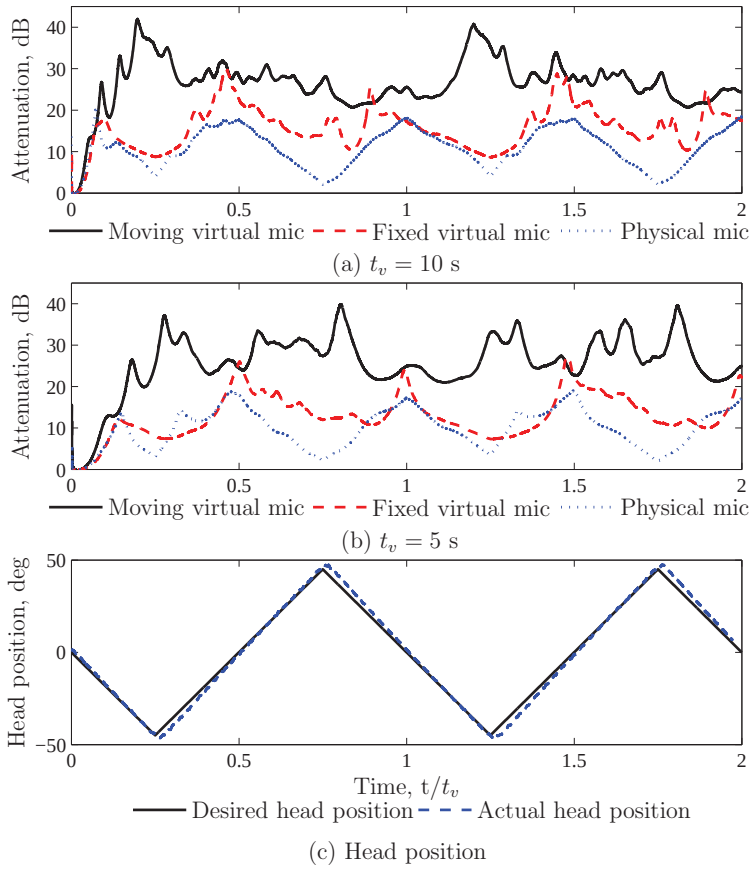

Figure B.2: Tonal attenuation achieved off resonance at 510 Hz with the remote moving microphone technique for a three-dimensional sound field. Control profiles are shown for active noise control at the moving virtual microphone, a virtual microphone spatially fixed at $\theta = 0°$, and the physical microphone, for a period of rotation (a) $t_v = 10$ s; (b) $t_v = 5$ s; and (c) head position.

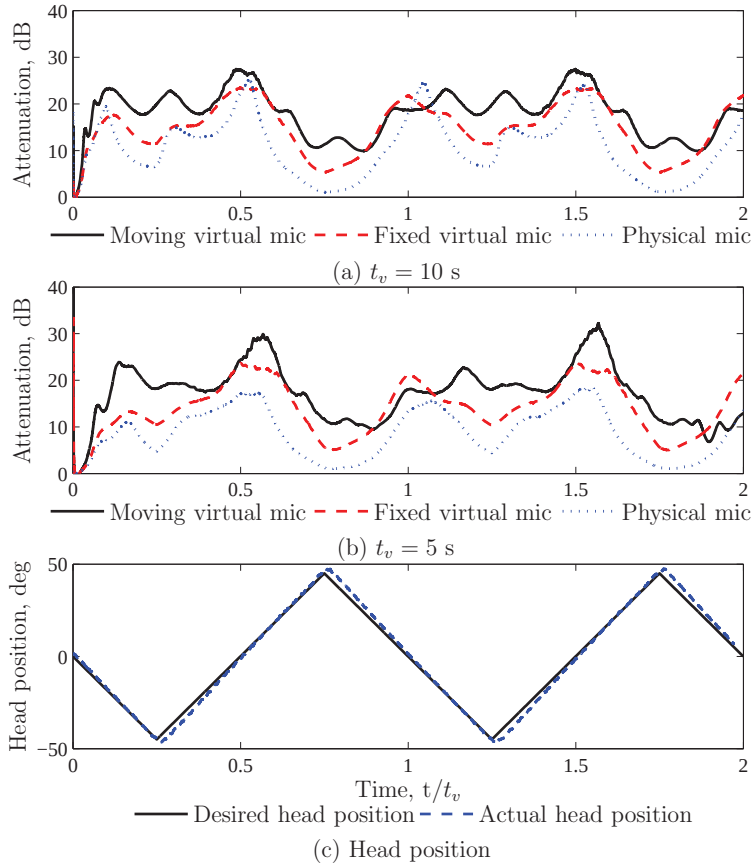

Figure B.3: Tonal attenuation achieved at the 525 Hz resonance with the remote moving microphone technique for a three-dimensional sound field after modifying the sound field. Control profiles are shown for active noise control at the moving virtual microphone, a virtual microphone spatially fixed at $\theta = 0°$, and the physical microphone, for a period of rotation (a) $t_v = 10$ s; (b) $t_v = 5$ s; and (c) head position.

with the remote moving microphone technique after modifying the sound field. The attenuation achieved at the moving virtual location is shown at the 525 Hz resonance and off resonance at 510 Hz in Figs. B.3 and B.4 respectively. Control profiles are shown for active noise control at the moving virtual microphone, a fixed virtual microphone located at the ear of the artificial head when $\theta_h = 0°$, and the fixed physical microphone. The control performance at the ear of the artificial head is shown for the period of head rotation of $t_v = 10$ s in part (a) of Figs. B.3 and B.4 and $t_v = 5$ s in part (b) of Figs. B.3 and B.4. Part (c) of Figs. B.3 and B.4 shows the desired trajectory of the artificial head and of the moving virtual microphone, in degrees, compared to the actual controlled head position.

At the 525 Hz resonance in the modified sound field, with $t_v = 10$ s, active noise

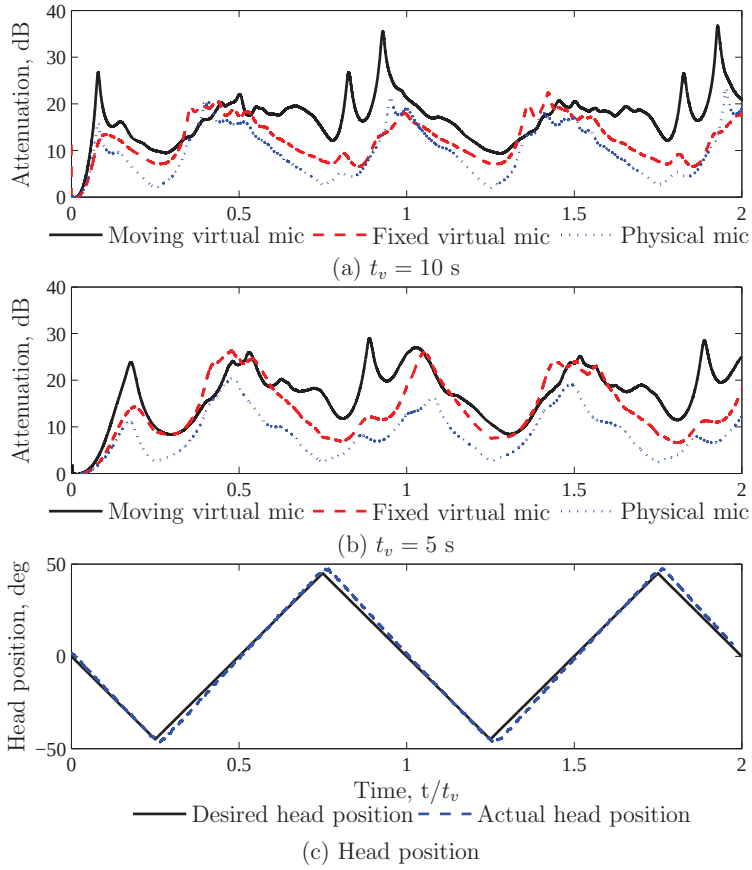

Figure B.4: Tonal attenuation achieved off resonance at 510 Hz with the remote moving microphone technique for a three-dimensional sound field after modifying the sound field. Control profiles are shown for active noise control at the moving virtual microphone, a virtual microphone spatially fixed at $\theta = 0°$, and the physical microphone, for a period of rotation (a) $t_v = 10$ s; (b) $t_v = 5$ s; and (c) head position.

control at the moving virtual microphone achieves between 10 dB and 29 dB of attenuation at the ear of the artificial head, as shown in Fig. B.3 (a). Minimising the fixed virtual error signal in the modified sound field achieves a maximum attenuation of 23 dB at the ear of the artificial head when $\theta_h = 0°$ and a minimum attenuation of 6 dB when $\theta_h = 45°$. Active noise control at the physical microphone achieves 24 dB of attenuation at the ear of the artificial head when $\theta_h = 0°$ and only 1 dB of attenuation when $\theta_h = 45°$. When the period of head rotation is reduced to $t_v = 5$ s, Fig. B.3 (b) shows that minimising the moving virtual error signal results in attenuation of between 10 dB and 30 dB being achieved at the ear of the artificial head in the modified sound field.

Off resonance with $t_v = 10$ s, active noise control at the moving virtual microphone in the modified sound field achieves an attenuation of between 10 dB and 39 dB at the ear of the artificial head, as shown in Fig. B.4 (a). Minimising the fixed virtual error signal in the modified sound field achieves a maximum attenuation of 21 dB at the ear of the artificial head when $\theta_h = 0°$ and a minimum attenuation of 8 dB when $\theta_h = 45°$. Active noise control at the physical microphone results in 20 dB of attenuation at the ear of the artificial head when $\theta_h = 0°$ and only 2 dB of attenuation when $\theta_h = 45°$. When the period of head rotation is reduced to $t_v = 5$ s, Fig. B.4 (b) shows that minimising the moving virtual error signal in the modified sound field results in attenuation of between 9 dB and 29 dB being achieved at the ear of the artificial head. This is still an improvement in control performance compared to active noise control at either the fixed virtual or physical microphone where the minimum attenuation levels are 7 dB and 2 dB respectively when $\theta_h = 45°$.

B.2 The adaptive LMS moving virtual microphone technique for a three-dimensional sound field

Figs. B.5 - B.8 (Figs. 4.14 - 4.17 in Section 4.3.2) show the attenuation achieved at the moving virtual location with the adaptive LMS moving virtual microphone technique at the 525 Hz resonance for $M_a = 3$ physical microphones being in linear formation perpendicular to the head, linear formation parallel to the head, triangular formation and $M_a = 4$ physical microphones in tetrahedral formation respectively. Control profiles are shown for active noise control at the moving virtual microphone, a fixed virtual microphone located at the ear of the artificial head when $\theta_h = 0°$, and

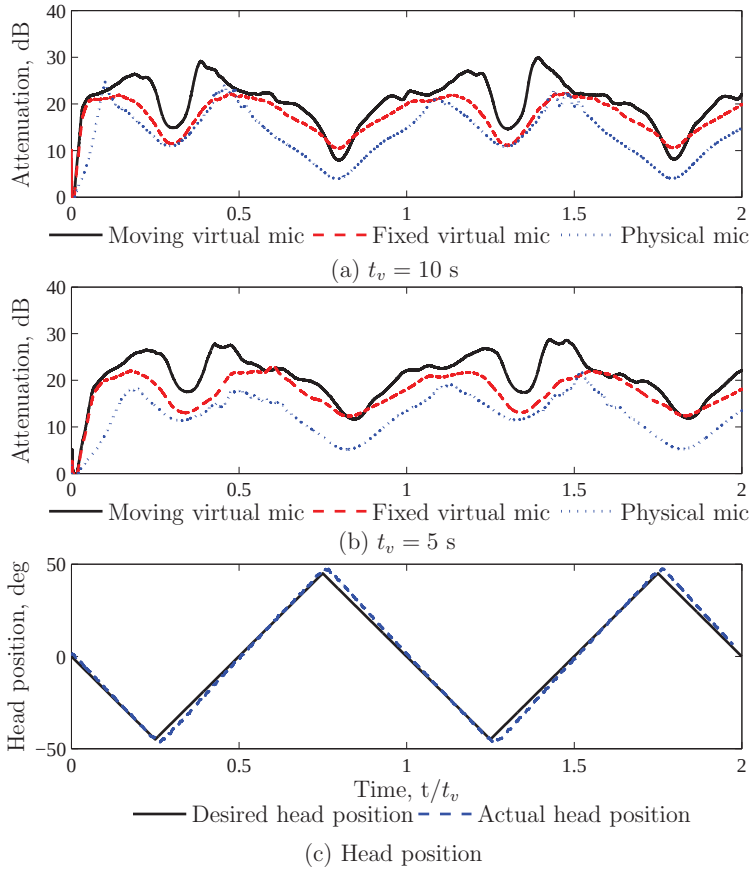

(a) $t_v = 10$ s

(b) $t_v = 5$ s

(c) Head position

Figure B.5: Tonal attenuation achieved at the 525 Hz resonance with the adaptive LMS moving virtual microphone technique for a three-dimensional sound field when $M_a = 3$ physical microphones are in linear perpendicular configuration. Control profiles are shown for active noise control at the moving virtual microphone, a virtual microphone spatially fixed at $\theta = 0°$, and the physical microphone, for a period of rotation (a) $t_v = 10$ s; (b) $t_v = 5$ s; and (c) head position.

a fixed physical microphone located 4 cm from the ear when $\theta_h = 0°$. The control performance at the ear of the artificial head is shown for the period of head rotation of $t_v = 10$ s in part (a) of Figs. B.5 - B.8 and $t_v = 5$ s in part (b) of Figs. B.5 - B.8. Part (c) of Figs. B.5 - B.8 shows the desired trajectory of the artificial head and of the moving virtual microphone, in degrees, compared to the actual controlled head position. As previously stated, the transient behaviour seen in Figs. B.5 - B.8 at time $t/t_v = 0$ s for both $t_v = 5$ s and $t_v = 10$ s, is caused by the controller initialising.

Fig. B.5 shows the attenuation achieved at the ear of the rotating artificial head when $M_a = 3$ physical microphones are arranged in linear formation perpendicular to the head motion. When $t_v = 10$ s, active noise control at the moving virtual

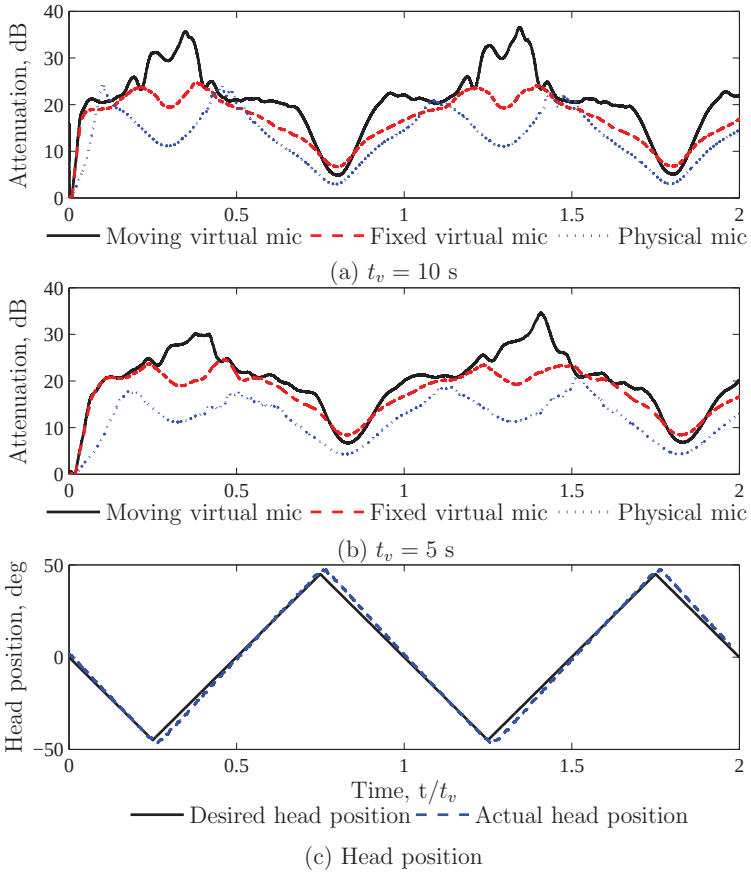

Figure B.6: Tonal attenuation achieved at the 525 Hz resonance with the adaptive LMS moving virtual microphone technique for a three-dimensional sound field when $M_a = 3$ physical microphones are in linear parallel configuration. Control profiles are shown for active noise control at the moving virtual microphone, a virtual microphone spatially fixed at $\theta = 0°$, and the physical microphone, for a period of rotation (a) $t_v = 10$ s; (b) $t_v = 5$ s; and (c) head position.

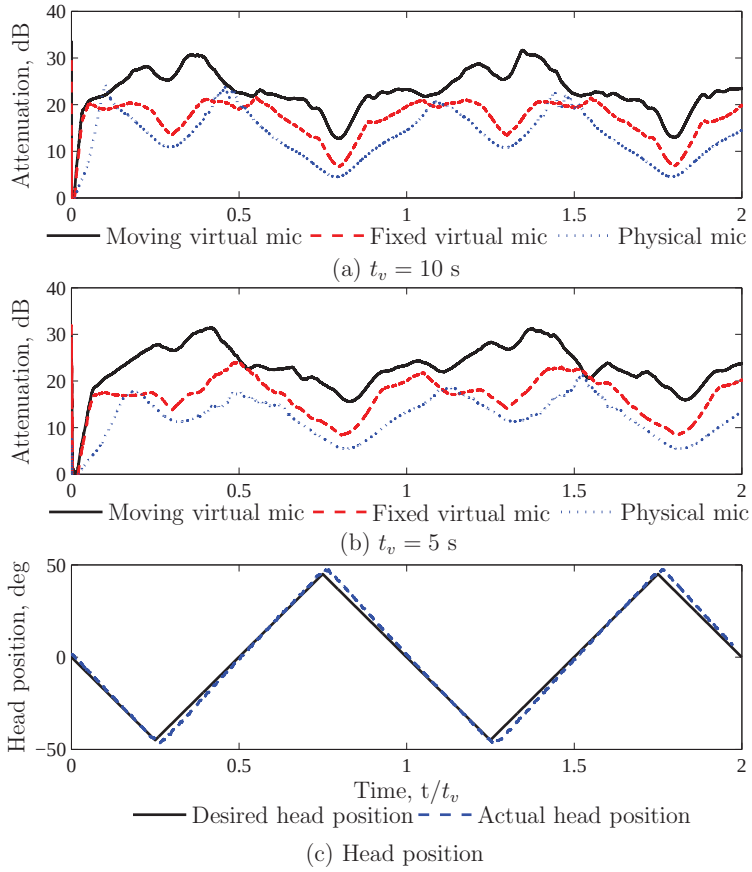

Figure B.7: Tonal attenuation achieved at the 525 Hz resonance with the adaptive LMS moving virtual microphone technique for a three-dimensional sound field when $M_a = 3$ physical microphones are in triangular configuration. Control profiles are shown for active noise control at the moving virtual microphone, a virtual microphone spatially fixed at $\theta = 0°$, and the physical microphone, for a period of rotation (a) $t_v = 10$ s; (b) $t_v = 5$ s; and (c) head position.

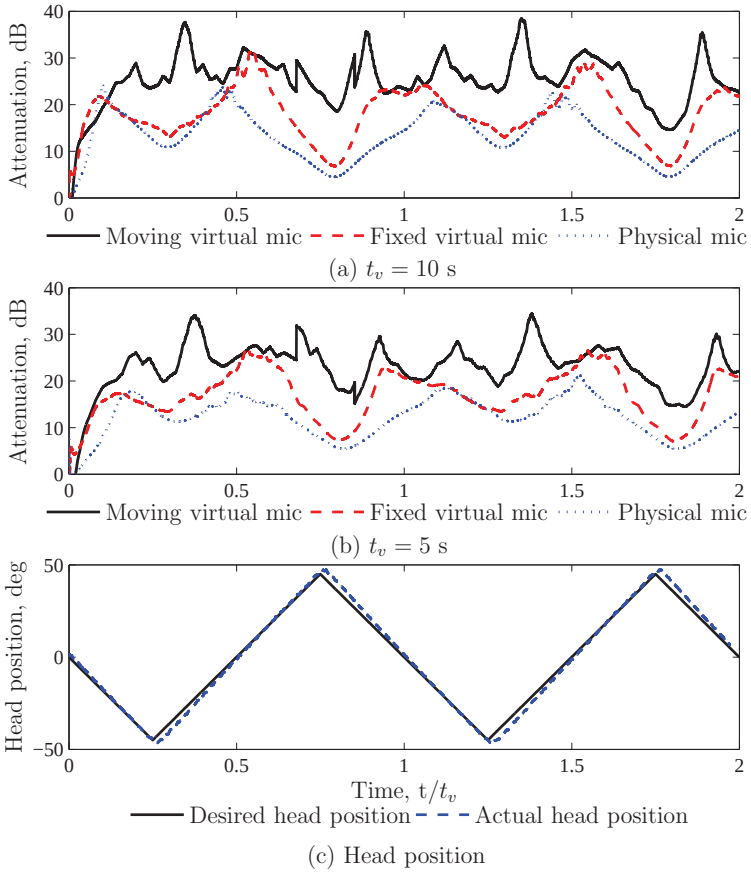

Figure B.8: Tonal attenuation achieved at the 525 Hz resonance with the adaptive LMS moving virtual microphone technique for a three-dimensional sound field when $M_a = 4$ physical microphones are in tetrahedral configuration. Control profiles are shown for active noise control at the moving virtual microphone, a virtual microphone spatially fixed at $\theta = 0°$, and the physical microphone, for a period of rotation (a) $t_v = 10$ s; (b) $t_v = 5$ s; and (c) head position.

microphone achieves between 9 dB and 30 dB of attenuation at the ear of the artificial head, as shown in Fig. B.5 (a). Minimising the fixed virtual error signal achieves a maximum attenuation of 23 dB at the ear of the artificial head when $\theta_h = 0°$ and a minimum attenuation of 12 dB when $\theta_h = 45°$. Active noise control at the physical microphone achieves 24 dB of attenuation at the ear of the artificial head when $\theta_h = 0°$ and only 4 dB of attenuation when $\theta_h = 45°$. When the period of head rotation is reduced to $t_v = 5$ s, Fig. B.5 (b) shows that minimising the moving virtual error signal results in attenuation of between 12 dB and 28 dB being achieved at the ear of the artificial head. This is a slight improvement in control performance compared to active noise control at either the fixed virtual or physical microphone where attenuation levels again fall to 13 dB and 6 dB respectively when $\theta_h = 45°$.

The attenuation achieved at the ear of the rotating artificial head when $M_a = 3$ physical microphones are arranged in linear formation parallel to the head motion is shown in Fig. B.6. When $t_v = 10$ s, Fig. B.6 (a) demonstrates that active noise control at the moving virtual microphone achieves between 5 dB and 36 dB of attenuation at the moving virtual location. This is compared to minimising either the fixed virtual or the physical error signal where maximum attenuation levels of 23 dB and 24 dB respectively are achieved at the ear of rotating artificial head. When the period of head rotation is reduced to $t_v = 5$ s, Fig. B.6 (b) shows that active noise control at the moving virtual microphone results in attenuation of between 5 dB and 34 dB being achieved at the ear of the artificial head. Minimising the moving virtual error signal achieves greater attenuation at the ear of the rotating artificial head compared to active noise control at either the fixed virtual or physical microphone where attenuation levels again fall to 10 dB and 5 dB respectively when $\theta_h = 45°$.

Fig. B.7 shows the attenuation achieved at the ear of the rotating artificial head when $M_a = 3$ physical microphones are arranged in triangular formation around the head. Fig. B.7 (a) shows that when $t_v = 10$ s, active noise control at the moving virtual microphone achieves between 15 dB and 31 dB of attenuation at the ear of the rotating artificial head. This is an increase in control performance compared to minimising the fixed virtual error signal where a maximum attenuation of 20 dB is achieved at the moving virtual location when $\theta_h = 0°$ and a minimum attenuation of 9 dB is achieved when $\theta_h = 45°$. Active noise control at the physical microphone generates 24 dB of attenuation at the ear of the artificial head when $\theta_h = 0°$ and only 5 dB of attenuation when $\theta_h = 45°$. When the period of head rotation is reduced to

$t_v = 5$ s, Fig. B.7 (b) shows that minimising the moving virtual error signal results in attenuation of between 18 dB and 31 dB being achieved at the ear of the rotating artificial head. This is an improvement in control performance compared to active noise control at either the fixed virtual or physical microphone where attenuation levels again fall to 9 dB and 6 dB respectively when $\theta_h = 45°$.

The attenuation achieved at the moving virtual location when $M_a = 4$ physical microphones are arranged in tetrahedral formation is shown in Fig. B.8. When $t_v = 10$ s, minimising the moving virtual error signal achieves between 16 dB and 39 dB of attenuation at the ear of the rotating artificial head as shown in Fig. B.8 (a). This is significant increase in control performance compared to active noise control at the fixed virtual microphone where a maximum attenuation of 31 dB is achieved the ear of the artificial head when $\theta_h = 0°$ and a minimum attenuation of 9 dB is achieved when $\theta_h = 45°$. Active noise control at the physical microphone only achieves 24 dB of attenuation at the ear of the artificial head when $\theta_h = 0°$ and 6 dB of attenuation when $\theta_h = 45°$. When the period of head rotation is reduced to $t_v = 5$ s, Fig. B.8 (b) shows that minimising the moving virtual error signal results in attenuation of between 15 dB and 37 dB being achieved at the ear of the artificial head. This is still a significant improvement in control performance compared to minimising the fixed virtual or physical microphone signal where attenuation levels again fall to 7 dB and 6 dB respectively when $\theta_h = 45°$.

The performance of the adaptive LMS moving virtual microphone technique off resonance at 510 Hz, with $M_a = 4$ physical microphones in tetrahedral formation, is shown in Fig. B.9 (Fig. 4.22 in Section 4.3.2). Control profiles are shown for active noise control at the moving virtual microphone, a fixed virtual microphone located at the ear of the artificial head when $\theta_h = 0°$, and a physical microphone 4 cm from the ear when $\theta_h = 0°$. The control performance at the ear of the rotating artificial head is shown for the period of head rotation of $t_v = 10$ s in Fig. B.9 (a) and $t_v = 5$ s in Fig. B.9 (b). Fig. B.9 demonstrates that off resonance, for both periods of head motion, active noise control at the moving virtual microphone outperforms minimising the fixed virtual or physical error signal. When $t_v = 10$ s, minimising the moving virtual error signal achieves between 20 dB and 38 dB of attenuation at the ear of the artificial head as shown in Fig. B.9 (a). Minimising the fixed virtual error signal achieves a maximum attenuation of 24 dB at the ear of the artificial head when $\theta_h = 0°$ and a minimum attenuation of 10 dB when $\theta_h = 45°$. Active noise control at the physical microphone achieves 17 dB of attenuation at the ear of the artificial head when $\theta_h = 0°$ and only 2 dB of attenuation when $\theta_h = 45°$.

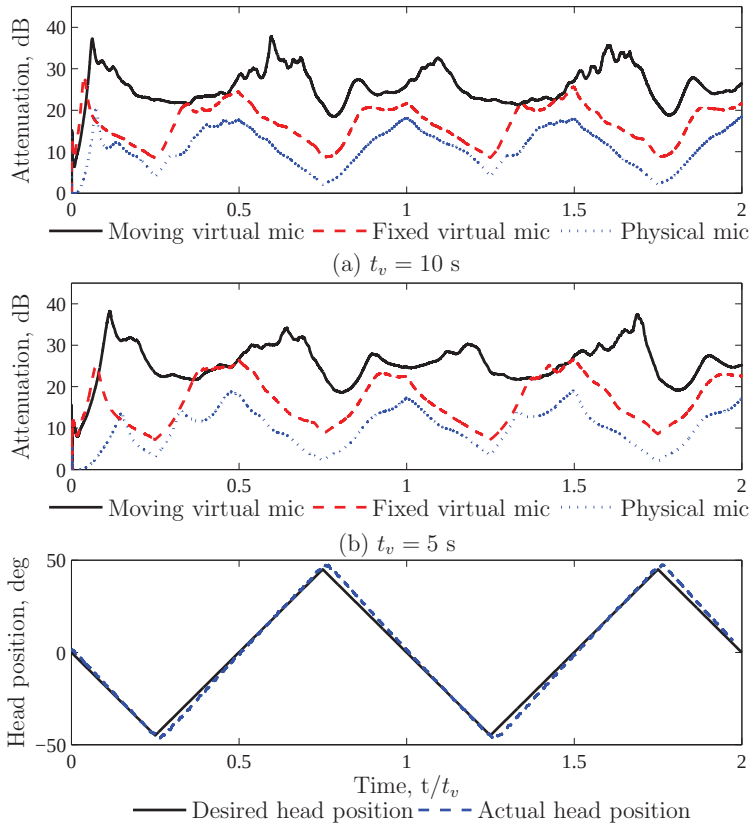

(a) $t_v = 10$ s

(b) $t_v = 5$ s

(c) Head position

Figure B.9: Tonal attenuation achieved off resonance at 510 Hz with the adaptive LMS moving virtual microphone technique for a three-dimensional sound field when $M_a = 4$ physical microphones are in tetrahedral configuration. Control profiles are shown for active noise control at the moving virtual microphone, a virtual microphone spatially fixed at $\theta = 0°$, and the physical microphone, for a period of rotation (a) $t_v = 10$ s; (b) $t_v = 5$ s; and (c) head position.

When the period of head rotation is reduced to $t_v = 5$ s, Fig. B.9 (b) shows that minimising the moving virtual error signal results in attenuation of between 20 dB and 39 dB being achieved at the ear of the moving virtual location. This is an improvement in control performance compared to active noise control at either the fixed virtual or physical microphone where attenuation levels again fall to 10 dB and 2 dB respectively when $\theta_h = 45°$.

B.2.1 Robustness of the adaptive LMS moving virtual microphone technique for a three-dimensional sound field

Figs. B.10 and B.11 (Figs. 4.23 and 4.24 in Section 4.3.2.1) show the performance of the active noise control system in generating a zone of quiet at the ear of the rotating artificial head with the adaptive LMS moving virtual microphone technique in a modified sound field. Arranging $M_a = 4$ physical microphones in tetrahedral formation was shown to generate the most accurate estimate of the moving virtual error signal and therefore, the robustness of the adaptive LMS moving virtual microphone technique is only examined for this configuration of physical sensors. The attenuation achieved at the moving virtual location is shown at the 525 Hz resonance and off resonance at 510 Hz in Figs. B.10 and B.11 respectively. Control profiles are shown for active noise control at the moving virtual microphone, a fixed virtual microphone located at the ear of the artificial head when $\theta_h = 0°$, and the fixed physical microphone. The control performance at the ear of the artificial head is shown for the period of head rotation of $t_v = 10$ s in part (a) of Figs. B.10 and B.11 and $t_v = 5$ s in part (b) of Figs. B.10 and B.11. Part (c) of Figs. B.10 and B.11 shows the desired trajectory of the artificial head and of the moving virtual microphone, in degrees, compared to the actual controlled head position.

At the 525 Hz resonance in the modified sound field, with $t_v = 10$ s, active noise control at the moving virtual microphone achieves between 9 dB and 30 dB of attenuation at the ear of the artificial head, as shown in Fig. B.10 (a). Minimising the fixed virtual error signal in the modified sound field achieves a maximum attenuation of 30 dB at the ear of the artificial head when $\theta_h = 0°$ and a minimum attenuation of 6 dB when $\theta_h = 45°$. Active noise control at the physical microphone achieves 29 dB of attenuation at the ear of the artificial head when $\theta_h = 0°$ and only 1 dB of attenuation when $\theta_h = 45°$. When the period of head rotation is reduced to $t_v = 5$ s, Fig. B.10 (b) shows that minimising the moving virtual error signal results in attenuation of between 12 dB and 28 dB being achieved at the ear of the artificial head. Minimising the moving virtual error signal in the modified sound field does show an improvement in control performance compared to active noise control at either the fixed virtual or physical microphone where attenuation levels again fall to 5 dB and 1 dB respectively when $\theta_h = 45°$.

Off resonance with $t_v = 10$ s, active noise control at the moving virtual microphone in the modified sound field achieves an attenuation of between 12 dB and 30

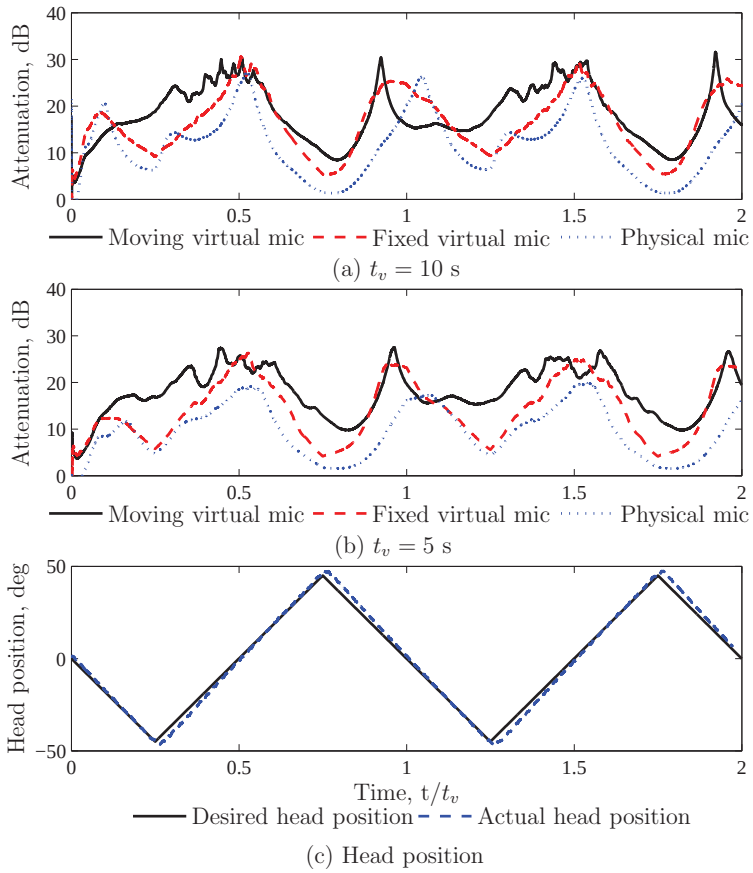

Figure B.10: Tonal attenuation achieved at the 525 Hz resonance with the adaptive LMS moving virtual microphone technique for a three-dimensional sound field after modifying the sound field. Results are shown for $M_a = 4$ physical microphones arranged in tetrahedral formation. Control profiles are shown for active noise control at the moving virtual microphone, a virtual microphone spatially fixed at $\theta = 0°$, and the physical microphone, for a period of rotation (a) $t_v = 10$ s; (b) $t_v = 5$ s; and (c) head position.

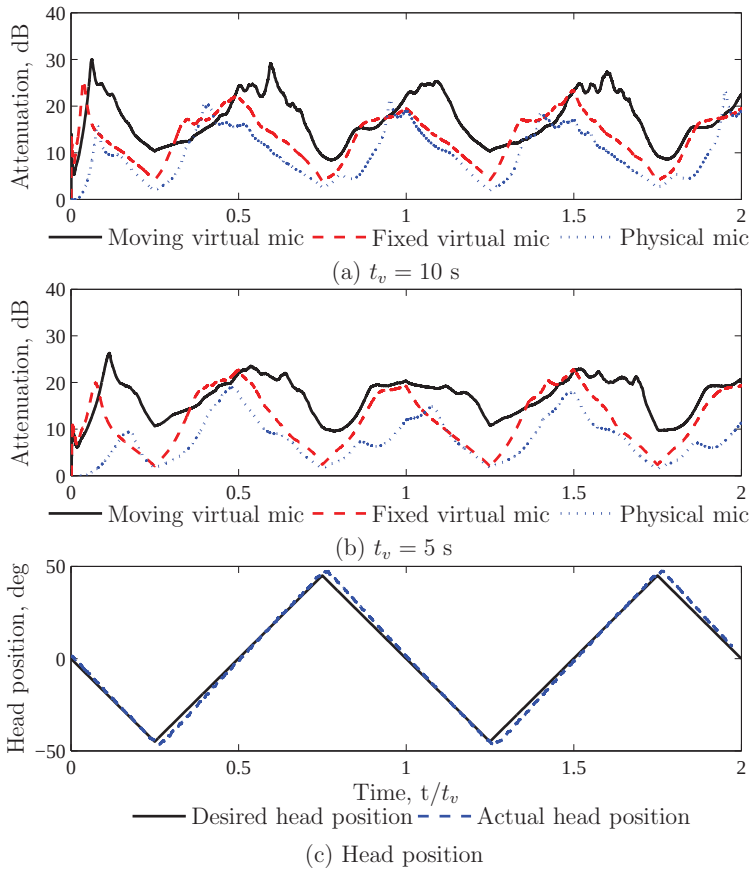

(a) $t_v = 10$ s

(b) $t_v = 5$ s

(c) Head position

Figure B.11: Tonal attenuation achieved off resonance at 510 Hz with the adaptive LMS moving virtual microphone technique for a three-dimensional sound field after modifying the sound field. Results are shown for $M_a = 4$ physical microphones arranged in tetrahedral formation. Control profiles are shown for active noise control at the moving virtual microphone, a virtual microphone spatially fixed at $\theta = 0°$, and the physical microphone, for a period of rotation (a) $t_v = 10$ s; (b) $t_v = 5$ s; and (c) head position.

dB at the ear of the artificial head, as shown in Fig. B.11 (a). This figure also shows that minimising the fixed virtual error signal in the modified sound field achieves a maximum attenuation of 26 dB at the ear of the artificial head when $\theta_h = 0°$ and a minimum attenuation of 5 dB when $\theta_h = 45°$. Active noise control at the physical microphone results in 21 dB of attenuation at the ear of the artificial head when $\theta_h = 0°$ and only 2 dB of attenuation when $\theta_h = 45°$. When the period of head rotation is reduced to $t_v = 5$ s, Fig. B.11 (b) shows that minimising the moving virtual error signal in the modified sound field results in attenuation of between 12 dB and 28 dB being achieved at the ear of the artificial head. This is an improvement in control performance compared to active noise control at either the fixed virtual or physical microphone where the minimum attenuation levels are 2 dB when $\theta_h = 45°$.

B.3 The Stochastically Optimal Tonal Diffuse Field (SOTDF) moving virtual sensing method for a three-dimensional sound field

Figs. B.12 - B.14 (Figs. 4.25 - 4.27 in Section 4.3.3) show the average attenuation achieved at the moving virtual location with the SOTDF moving virtual sensing technique at the 525 Hz resonance. Results are given for the virtual quantities being estimated using the measured pressure and pressure gradient at a point, the measured pressures at two points, and the measured pressures at three points respectively. The control profiles in Figs. B.12 - B.14 have been generated by averaging the results of active noise control at 10 different cavity locations. In Figs. B.12 - B.14, the average control profiles are shown for active noise control at the moving virtual microphone, a fixed virtual microphone located at the ear of the rotating artificial head when $\theta_h = 0°$, and the fixed physical microphone located 4 cm from the ear when $\theta_h = 0°$. The average control performance at the ear of the rotating artificial head is shown for the period of head rotation of $t_v = 10$ s in part (a) of Figs. B.12 - B.14 and $t_v = 5$ s in part (b) of Figs. B.12 - B.14. Part (c) of Figs. B.12 - B.14 shows the desired trajectory of the artificial head and of the moving virtual microphone, in degrees, compared to the actual controlled head position. Again, the transient behaviour seen in Figs. B.12 - B.14 at time $t/t_v = 0$ s for both $t_v = 5$ s and $t_v = 10$ s, is caused by the controller initialising.

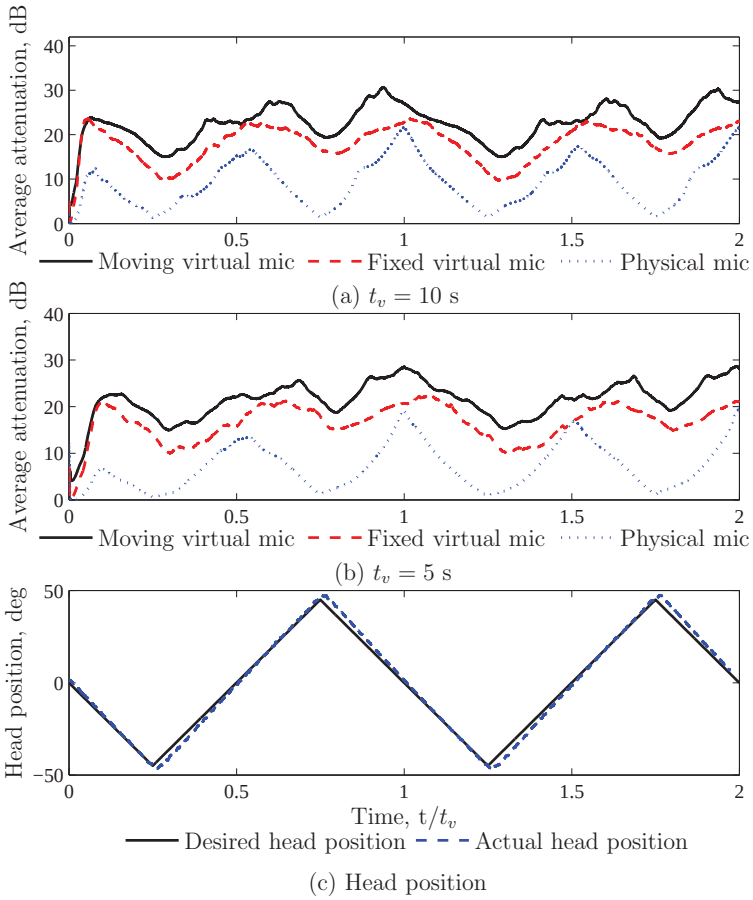

Figure B.12: The average tonal attenuation achieved at the 525 Hz resonance with the SOTDF moving virtual sensing method using the measured pressure and pressure gradient at a point. Control profiles are shown for active noise control at the moving virtual microphone, a virtual microphone spatially fixed at $\theta = 0°$, and the physical microphone, for a period of rotation (a) $t_v = 10$ s; (b) $t_v = 5$ s; and (c) head position.

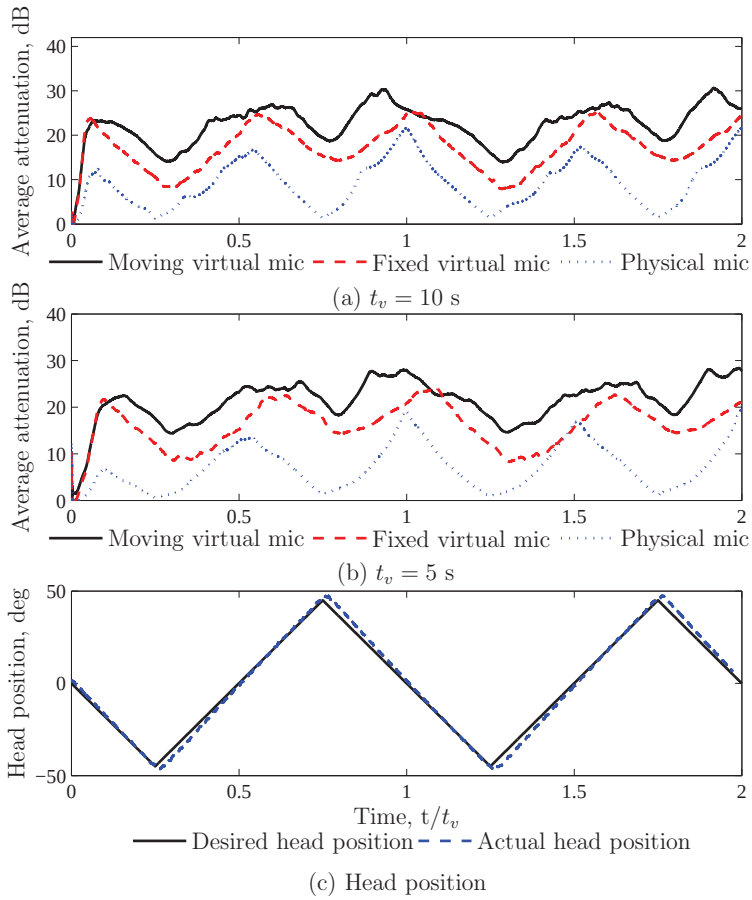

Figure B.13: The average tonal attenuation achieved at the 525 Hz resonance with the SOTDF moving virtual sensing method using the measured pressures at two points. Control profiles are shown for active noise control at the moving virtual microphone, a virtual microphone spatially fixed at $\theta = 0°$, and the physical microphone, for a period of rotation (a) $t_v = 10$ s; (b) $t_v = 5$ s; and (c) head position.

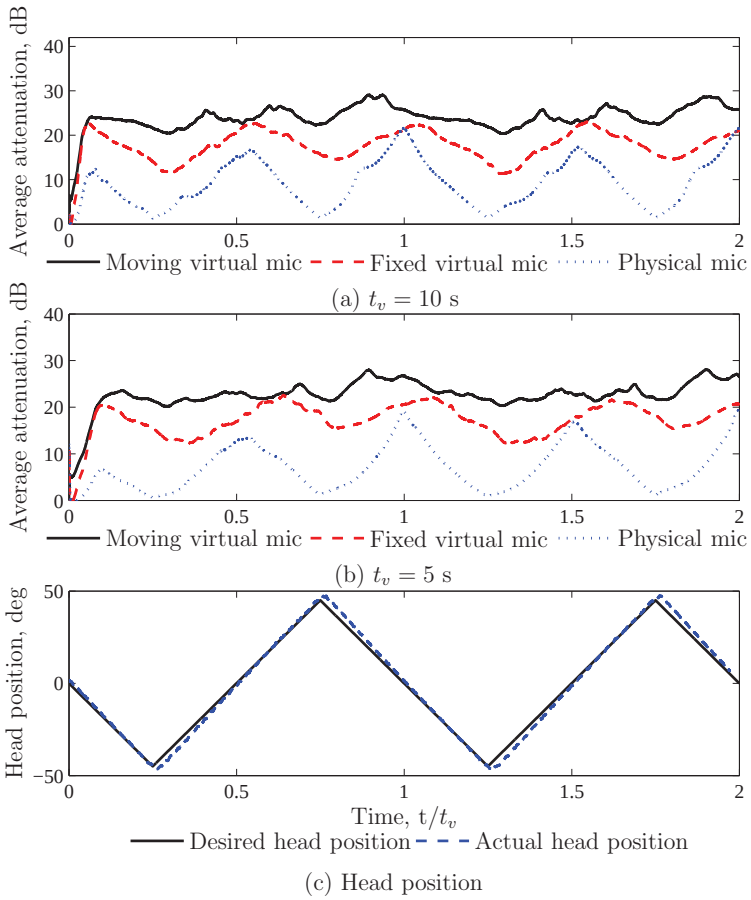

Figure B.14: The average tonal attenuation achieved at the 525 Hz resonance with the SOTDF moving virtual sensing method using the measured pressures at three points. Control profiles are shown for active noise control at the moving virtual microphone, a virtual microphone spatially fixed at $\theta = 0°$, and the physical microphone, for a period of rotation (a) $t_v = 10$ s; (b) $t_v = 5$ s; and (c) head position.

Fig. B.12 shows the average attenuation achieved at the ear of the rotating artificial head when the virtual quantities are estimated using the measured pressure and pressure gradient at a point. When $t_v = 10$ s, active noise control at the moving virtual microphone achieves an average attenuation of between 17 dB and 31 dB at the ear of the rotating artificial head as shown in Fig. B.12 (a). This is a significant improvement in control performance compared to minimising the fixed virtual error signal where average attenuation levels of between 11 dB and 24 dB are achieved at the ear of the rotating artificial head. In comparison, active noise control at the physical microphone only achieves an average attenuation of 20 dB at the ear of the artificial head when $\theta_h = 0^\circ$ and 1 dB when $\theta_h = 45^\circ$. When the period of head rotation is reduced to $t_v = 5$ s, Fig. B.12 (b) shows that minimising the moving virtual error signal results in an average attenuation of between 17 dB and 29 dB being achieved at the moving virtual location. This is again an improvement in control performance compared to active noise control at either the fixed virtual or physical microphone where the average attenuation levels again fall to 10 dB and 1 dB respectively when $\theta_h = 45^\circ$.

The average attenuation achieved at the ear of the rotating artificial head when the virtual quantities are estimated using the measured pressures at two points is shown in Fig. B.13. When $t_v = 10$ s, active noise control at the moving virtual microphone achieves an average attenuation of between 16 dB and 31 dB at the ear of the rotating artificial head, as shown in Fig. B.13 (a). Minimising the fixed virtual error signal achieves a maximum average attenuation level of 25 dB at the ear of the artificial head when $\theta_h = 0^\circ$ and a minimum average attenuation level of 7 dB when $\theta_h = 45^\circ$. In comparison, active noise control at the physical microphone achieves average attenuation levels of between 20 dB and 1 dB at the ear of the rotating artificial head. When the period of head rotation is reduced to $t_v = 5$ s, Fig. B.13 (b) shows that minimising the moving virtual error signal results in an average attenuation level of between 15 dB and 29 dB being achieved at the ear of the rotating artificial head. This is an improvement in the attenuation achieved at the ear of the rotating artificial head with active noise control at either the fixed virtual or physical microphone where the average attenuation levels again fall to 9 dB and 1 dB respectively when $\theta_h = 45^\circ$.

Fig. B.14 shows the average attenuation achieved at the ear of the rotating artificial head when the virtual quantities are estimated using the measured pressures at three points. Fig. B.14 (a) shows that when $t_v = 10$ s, active noise control at the moving virtual microphone achieves an average attenuation of between 22 dB

and 30 dB at the ear of the artificial head. Minimising the fixed virtual error signal generates a maximum average attenuation of 24 dB at the ear of the artificial head when $\theta_h = 0°$ and a minimum average attenuation of 12 dB when $\theta_h = 45°$. In comparison, active noise control at the physical microphone achieves only an average attenuation level of between 20 dB and 1 dB at the ear of the rotating artificial head. When the period of head rotation is reduced to $t_v = 5$ s, Fig. B.14 (b) shows that minimising the moving virtual error signal results in an average attenuation of between 21 dB and 29 dB being achieved at the ear of the artificial head. This is an improvement in control performance compared to active noise control at either the fixed virtual or physical microphone where the average attenuation levels again fall to 12 dB and 1 dB respectively when $\theta_h = 45°$.

The performance of the SOTDF moving virtual sensing method off resonance at 510 Hz is shown in Fig. B.15 (Fig. 4.37 in Section 4.3.3). In this figure, the moving and fixed virtual error signals have been estimated using the measured pressures at three points. This configuration of physical sensors was selected as it was shown to generate the greatest control performance at the moving virtual location. Control profiles are shown for active noise control at the moving virtual microphone, a fixed virtual microphone located at the ear of the artificial head when $\theta_h = 0°$, and a fixed physical microphone 4 cm from the ear when $\theta_h = 0°$. The control performance at the ear of the rotating artificial head is shown for the period of head rotation of $t_v = 10$ s in Fig. B.15 (a) and $t_v = 5$ s in Fig. B.15 (b). Fig. B.15 demonstrates that off resonance, for both periods of head motion, active noise control at the moving virtual microphone outperforms minimising the fixed virtual or physical error signal. When $t_v = 10$ s, minimising the moving virtual error signal achieves an average of between 14 dB and 28 dB of attenuation at the ear of the artificial head as shown in Fig. B.15 (a). Minimising the fixed virtual error signal achieves a maximum average attenuation of 19 dB at the ear of the artificial head when $\theta_h = 0°$ and a minimum average attenuation of 9 dB when $\theta_h = 45°$. Active noise control at the physical microphone achieves an average 19 dB of attenuation at the ear of the artificial head when $\theta_h = 0°$ and only 1 dB of attenuation on average when $\theta_h = 45°$. When the period of head rotation is reduced to $t_v = 5$ s, Fig. B.15 (b) shows that minimising the moving virtual error signal results in an average attenuation of between 16 dB and 25 dB being achieved at the ear of the moving virtual location. This is an improvement in control performance compared to active noise control at either the fixed virtual or physical microphone where average attenuation levels again fall to 10 dB and 1 dB respectively when $\theta_h = 45°$.

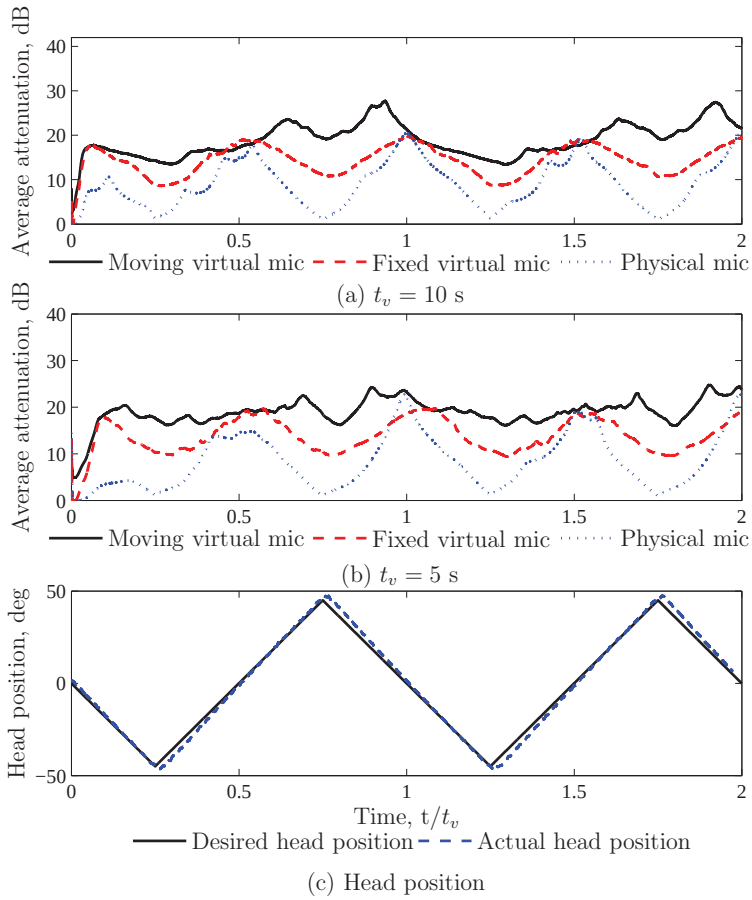

Figure B.15: Tonal attenuation achieved off resonance at 510 Hz with the SOTDF moving virtual sensing method using the measured pressures at three points. Control profiles are shown for active noise control at the moving virtual microphone, a virtual microphone spatially fixed at $\theta = 0°$, and the physical microphone, for a period of rotation (a) $t_v = 10$ s; (b) $t_v = 5$ s; and (c) head position.